J Physiol 589.8 (2011) pp 1957–1977

The Journal of Physiology

Cell type-specific and activity-dependent dynamics of action potential-evoked Ca^{2+} signals in dendrites of hippocampal inhibitory interneurons

Alesya Evstratova, Simon Chamberland and Lisa Topolnik

Axis of Cellular and Molecular Neuroscience, CRULRG, Department of Biochemistry, Microbiology and Bioinformatics, Université Laval, Québec, PQ, Canada

Non-technical summary Action potentials generated at the level of the cell body can propagate back to neuronal dendrites, where they activate different types of voltage-sensitive calcium channels and produce massive calcium influx. Although these calcium signals may control dendritic integration, their mechanisms, dynamic properties and role in different cell types remain largely unknown. We found that in dendrites of hippocampal interneurons, an inhibitory cell type involved in control of network excitability, specific types of calcium channels are present but are recruited in an activity-dependent manner. Furthermore, their activation produces calcium rises spatially restricted to proximal dendritic sites, where they control the efficacy of transmission at inhibitory synapses. The pathway by which this happens appears to constitute a negative feedback loop – increased firing activity of interneurons potentiates the inhibitory drive that they receive, thus decreasing the activity of interneurons further. This may have a profound effect on the recruitment of interneurons and network activity.

Abstract In most central neurons, action potentials (APs), generated in the initial axon segment, propagate back into dendrites and trigger considerable Ca^{2+} entry via activation of voltage-sensitive calcium channels (VSCCs). Despite the similarity in its underlying mechanisms, however, AP-evoked dendritic Ca^{2+} signalling often demonstrates a cell type-specific profile that is determined by the neuron dendritic properties. Using two-photon Ca^{2+} imaging in combination with patch-clamp whole-cell recordings, we found that in distinct types of hippocampal inhibitory interneurons Ca^{2+} transients evoked by backpropagating APs not only were shaped by the interneuron-specific properties of dendritic Ca^{2+} handling but also involved specific Ca^{2+} mechanisms that were regulated dynamically by distinct activity patterns. In dendrites of regularly spiking basket cells, AP-evoked Ca^{2+} rises were of large amplitude and fast kinetics; however, they decreased with membrane hyperpolarization or following high-frequency firing episodes. In contrast, AP-evoked Ca^{2+} elevations in dendrites of Schaffer collateral-associated cells exhibited significantly smaller amplitude and slower kinetics, but increased with membrane hyperpolarization. These cell type-specific properties of AP-evoked dendritic Ca^{2+} signalling were determined by distinct endogenous buffer capacities of the interneurons examined and by specific types of VSCCs recruited by APs during different patterns of activity. Furthermore, AP-evoked Ca^{2+} transients summated efficiently during theta-like bursting and were associated with the induction of long-term potentiation at inhibitory synapses onto both types of interneurons. Therefore, the cell type-specific profile of AP-evoked dendritic Ca^{2+} signalling is shaped in an activity-dependent manner, such that the same pattern of hippocampal activity can be differentially translated into dendritic Ca^{2+} signals in different cell types. However, Cell

DOI: 10.1113/jphysiol.2010.204255

type-specific differences in Ca^{2+} signals can be 'smoothed out' by changes in neuronal activity, providing a means for common, cell-type-independent forms of synaptic plasticity.

(Received 16 December 2010; accepted after revision 22 February 2011; first published online 28 February 2011)
Corresponding author L. Topolnik: Axis of Cellular and Molecular Neuroscience, 2601 Ch. De La Canardière, CRULRG, Québec, PQ, G1J 2G3, Canada. Email: lisa.topolnik@crulrg.ulaval.ca

Abbreviations AP, action potential; AP-CaTs, action potential-evoked Ca^{2+} transients; BC, basket cell; CaMKII, calmodulin-dependent kinase II; CCK-IR, cholecystokinin-immunoreactive; CV, coefficient of variation; FS-BC, fast spiking basket cell; IN, interneuron; LTP, long-term potentiation; NGS, normal goat serum; O/A, stratum oriens/alveus; OGB-1, Oregon Green 488 BAPTA-1; PPR, paired-pulse ratio; PYR, stratum pyramidale, RAD, stratum radiatum; SC-AC, Schaffer collateral-associated cell; TBF, theta-burst firing; VSCC, voltage-sensitive calcium channel.

Introduction

When a neuron fires an action potential (AP), it does not simply transmit a signal along its axon to the postsynaptic target, but also sends it back to its own dendrites, activating specific membrane conductances and thus controlling the integrative properties of dendrites. Different types of voltage-sensitive calcium channels (VSCCs) are activated by backpropagating APs in neuronal dendrites and represent a major source of Ca^{2+} influx (Callaway & Ross, 1995; Yuste & Denk, 1995; Sabatini & Svoboda, 2000). The development of a two-photon Ca^{2+} imaging technique to monitor Ca^{2+} signalling in neuronal dendrites (Denk *et al.* 1995; Yuste & Denk, 1995; Sabatini & Svoboda, 2000; Sabatini *et al.* 2002) allowed the detailed investigation of the functional organization of dendritic Ca^{2+} and, therefore, a better understanding of its role in dendritic information processing. In inhibitory interneurons (INs), dendritic Ca^{2+} transients evoked by backpropagating APs (AP-CaTs) may exhibit cell type-specific properties due to specific endogenous Ca^{2+} binding capacities and active properties of their dendrites (Goldberg *et al.* 2003, 2004; Rozsa *et al.* 2004; Aponte *et al.* 2008). AP-evoked Ca^{2+} signalling plays a role in the induction of several forms of synaptic plasticity at both excitatory and inhibitory synapses in INs (Perez *et al.* 2001; Lei & McBain, 2002; Lapointe *et al.* 2004; Lamsa *et al.* 2005; Patenaude *et al.* 2005; Ali, 2007). These functions of AP-CaTs, however, require specific patterns of IN activity (e.g. burst firing, persistent depolarization). Thus, given that different modes of IN activity may be associated with activation of distinct Ca^{2+} mechanisms, it is important to elucidate their implication as well as their cell type-specific regulation by the activity itself. Despite the strong expression of different types of VSCCs in INs (Vinet & Sík, 2006), the role and regulation of VSCCs in IN dendrites remain largely unknown (Topolnik *et al.* 2009). Similarly, very little is currently known about the activity-dependent regulation of dendritic AP-CaTs (Yasuda *et al.* 2003; Scheuss *et al.* 2006). Activity-dependent slowing of AP-CaTs due to depression of Ca^{2+} extrusion via plasma membrane Ca^{2+} pumps and Na^{+}/Ca^{2+} exchangers was reported during high-frequency firing activity in CA1 pyramidal neurons (Scheuss *et al.* 2006). Furthermore, following high-frequency firing episodes, AP-CaTs undergo long-term depression, which is expressed as a decrease in the open probability of R-type VSCCs (Yasuda *et al.* 2003). Such activity-dependent regulation of AP-evoked dendritic Ca^{2+} signalling remains elusive in distinct types of hippocampal inhibitory INs that are differentially involved in hippocampal rhythmic activity, associated with specific spatial and cognitive tasks in animals and humans (O'Keefe & Recce, 1993; Soltesz & Deschênes, 1993; Csicsvari *et al.* 1998; Klausberger *et al.* 2003).

In this paper, we examined the properties, activity-dependent regulation and role in synaptic plasticity of Ca^{2+} transients associated with backpropagating APs in dendrites of two types of hippocampal inhibitory interneurons: regularly spiking basket cells and Schaffer collateral-associated cells.

Methods

Electrophysiology

All experiments were carried out in accordance with the animal welfare guidelines of the Animal Protection Committee of Université Laval. A total of 140 C57BL/6 mice (P15–30; mean age ± SD, 22 ± 3 days; Charles River, St Laurent, Québec, Canada) were used in this study. Animals were deeply anaesthetized with isoflurane and decapitated. Transverse hippocampal slices (300 μm) were prepared in ice-cold (0–4°C) 'cutting' solution containing (in mM): 250 sucrose, 2 KCl, 1.25 NaH_2PO_4, 26 $NaHCO_3$, 7 $MgSO_4$, 0.5 $CaCl_2$ and 10 glucose, saturated with 95% O_2–5% CO_2, pH 7.4; 320–340 mosmol l^{-1}. Slices were transferred to a heated (35°C) and oxygenated solution containing (in mM): 124 NaCl, 2.5 KCl, 1.25 NaH_2PO_4, 26 $NaHCO_3$, 3 $MgSO_4$, 1 $CaCl_2$ and 10 glucose for 30 min. After this they were kept at room temperature until use. During experiments, slices were continuously perfused (2 ml min^{-1}) with standard artificial cerebrospinal fluid (ACSF) containing (in mM): 124 NaCl, 2.5 KCl, 1.25 NaH_2PO_4, 26 $NaHCO_3$, 2 $MgSO_4$,

2 $CaCl_2$ and 10 glucose, saturated with 95% O_2–5% CO_2, pH 7.4, at near-physiological temperature (30–33°C).

Whole-cell recordings were obtained from INs in the stratum radiatum (RAD) in the CA1 area identified using a 40× water-immersion objective and Dodt infrared scanning gradient contrast (ISGC; Leica TCS SP5) optics. Recording pipettes (3.5–6 MΩ) were made from borosilicate glass capillaries (1B100F-4; World Precision Instruments Inc., Sarasota, FL, USA) pulled on a Flaming–Brown-type micropipette puller (P-97; Sutter Instrument Co., Novato, CA, USA). For whole-cell current-clamp recordings, the pipette solution contained the following (in mM): 130 $KMeSO_3$, 2 $MgCl_2$, 10 diNa-phosphocreatine, 10 Hepes, 2–4 ATP-Tris, 0.2 GTP-Tris and 0.15–0.2% biocytin, pH 7.25–7.35; 275–285 mosmol l^{-1}. Patch solution also contained either 50–200 μM Oregon Green 488 BAPTA-1 (OGB-1) or 300 μM Fluo-5F, to monitor calcium elevations, and 30 μM Alexa Fluor-594, to image neuronal morphology (all from Invitrogen).

Monosynaptic inhibitory postsynaptic currents (IPSCs) were evoked at 0.1 Hz via local stimulation with an electrode (2–3 MΩ) that was filled with ACSF, connected to a constant current isolation unit (A360LA; World Precision Instruments Inc., Sarasota, FL, USA) and positioned in the RAD. IPSCs were recorded at −50 mV in the presence of the NMDA and AMPA/kainate receptor antagonists DL-2-amino-5-phosphonopentanoic acid (DL-AP5; 50 μM) and 1,2,3,4-tetrahydro-6-nitro-2,3-dioxo-benzo[f]quinoxaline-7-sulfonamide (NBQX; 10 μM), respectively. Synaptic plasticity at inhibitory synapses was induced by repetitive theta-burst firing (TBF) at 5 Hz for 2 s (each burst consisting of 3 APs at 100 Hz), which was delivered three times at 30 s intervals. The paired-pulse ratio (PPR) of IPSCs was calculated as the ratio between the mean peak amplitude of the second response and the mean peak amplitude of the first response. The coefficient of variation (CV) of IPSCs was calculated as the ratio between the standard deviation of current amplitude and the mean current amplitude.

Two-photon Ca^{2+} imaging

Intracellular Ca^{2+} imaging was performed using a TCS SP5 two-photon laser-scanning microscope (Leica Microsystems Inc.) based on a Ti-Sapphire laser (Chameleon Ultra II; Coherent, Santa Clara, CA, USA; >3W, 140 fs pulses, 80 Hz repetition rate) tuned to 800 nm. A long-range water-immersion objective (40×; NA, 0.8) was used and emitted photons were collected in epifluorescence mode with external photomultiplier tubes.

Neurons were filled via the patch electrode for 20–30 min before imaging. Red fluorescence from Alexa Fluor-594 was used to locate dendrites of interest 10–200 μm from the soma (Fig. 2). Backpropagating APs were evoked by somatic current injection (0.8–1 nA, 2 ms). To measure Ca^{2+} signals, green and red fluorescence was collected during 500 Hz line scans across the dendrite (Fig. 2). Fluorescence changes were quantified as (1) increases in green fluorescence from baseline normalized to the red fluorescence ($\Delta G/R$) (Sabatini *et al.* 2002) or (2) changes in green fluorescence $F(t)$ from baseline F_0: $\Delta F/F(t) = (F(t) - F_0)/F_0$. Calcium concentration ($[Ca^{2+}]$) was calculated from $\Delta F/F$ or $\Delta G/R$ using a method that relies on the estimation of the fluorescence increase that would arise from a saturating $\Delta[Ca^{2+}]$ ($\Delta F/F_{max}$ or $\Delta G/R_{max}$) (Maravall *et al.* 2000; Sabatini *et al.* 2002; Yasuda *et al.* 2004).

$$\Delta[Ca^{2+}]/k_D = (\Delta F/F_{max} + 1) \times \left(1 - R_f^{-1}\right) \times (\Delta F/F/(\Delta F/F_{max} - \Delta F/F) \times \Delta F/F_{max}), \quad (1)$$

or

$$\Delta[Ca^{2+}]/k_D = (\Delta G/R_{max} + 1) \times \left(1 - R_f^{-1}\right) \times (\Delta G/R/(\Delta G/R_{max} - \Delta G/R) \times \Delta G/R_{max}), \quad (2)$$

where k_D is the constant of dissociation and R_f is the dynamic range of the indicator. Values used were $R_f = 6$ and $k_D = 206$ nM for OGB-1 (Maravall *et al.* 2000) and $R_f = 240$ and $k_D = 1280$ nM for Fluo-5F (Woodruff *et al.* 2002). $\Delta F/F_{max}$ or $\Delta G/R_{max}$ was determined from AP trains (60–80 Hz). For calculations of resting calcium concentration ($[Ca^{2+}]_0$, Maravall *et al.* 2000), measurements with OGB-1 were used exclusively, as Fluo-5F exhibits little fluorescence under basal conditions.

$$[Ca^{2+}]_0/k_D = ((1 - R_f^{-1})/\Delta F/F_{max}) - R_f^{-1} \quad (3)$$

To ensure that the high-affinity indicator OGB-1 was not saturated during the Ca^{2+} influx evoked by five APs, we compared the peak amplitude of CaTs evoked by five APs with that of a maximal response ($\Delta F/F_{max}$) evoked by high-frequency AP trains (60–80 Hz, 1 s). In all recorded INs, the peak amplitude of CaTs evoked by five APs was at least two times smaller than $\Delta F/F_{max}$, indicating the absence of dye saturation in response to five APs. Precautions were taken to avoid ejecting dye from the pipette into the slice, and no background correction was performed.

Buffer capacity measurement

Endogenous calcium buffer capacity (κ_S) was measured by competing endogenous buffers with increasing concentrations of exogenous buffer (50, 100 and 200 μM OGB-1; Fig. 3) (Helmchen *et al.* 1996; Maravall *et al.* 2000; Sabatini *et al.* 2002). $\Delta F/F_{AP}$ was converted to $[Ca^{2+}]_{AP}$

and the inverse peak of $[Ca^{2+}]_{AP}$ was plotted as a function of the exogenous buffer capacity (κ_B) (Fig. 3).

$$\kappa_B = (k_D \times [B]_t)/(k_D + [Ca^{2+}]_0) \times (k_D + [Ca^{2+}]_{AP}), \quad (4)$$

where $[B]_t$ is the total concentration of the buffer (Neher & Augustine, 1992). The relationships between $[Ca^{2+}]_{AP}{}^{-1}$ or τ_{decay} and κ_B were fitted by linear regression. κ_S was determined by extrapolating the fits to the x-intercept, whereas the amplitude of $\Delta[Ca^{2+}]_{AP}$ in conditions of 'zero' added buffer ($\kappa_B = 0$) was found by extrapolating the fits to the y-intercept (Fig. 3) (Helmchen *et al.* 1996). Ninety-five per cent confidence intervals (95% CIs) were determined using curve-fitting routines and error estimation in Igor Pro (WaveMetrics Inc., Lake Oswego, OR, USA) and were reported for each value.

Data acquisition and analysis

Image acquisition was performed using the Leica LAS software (Leica Microsystems Inc.). Physiological data acquisition (filtered at 2–3 kHz and digitized at 10 kHz) was performed using a data acquisition board (Digidata 1440 with Multiclamp 700B amplifier, Molecular Devices, Sunnyvale, CA, USA) and the Clampex 10.2 software (Molecular Devices). Data were analysed using Clampfit 10.2 (Molecular Devices) and Igor Pro (WaveMetrics).

Amplitudes of AP-evoked Ca^{2+} transients were measured at the peak of the waveform as averages over a 10 ms time window. The decay values were determined from double exponential fits and expressed as an amplitude-weighted average decay time constant. Summary data are shown as means ± SEM and analysed using Student's paired t test. Significance between groups was assessed using the unpaired t test or one-way ANOVA.

Anatomical reconstruction and immunohistochemistry

For anatomical reconstruction, neurons were filled with biocytin (Sigma) during whole-cell recordings. Slices with recorded cells were fixed overnight with 4% paraformaldehyde at 4°C. To reveal biocytin, slices were rinsed several times in Tris-buffered saline (TBS; pH 7.4, $t = 25$°C), treated with hydrogen peroxide (0.3%) for 30 min and permeabilized with 3% Triton X-100 in TBS for 1 h. To reduce non-specific background staining, the slices were then incubated for 30 min in TBS containing 10% normal goat serum (NGS) and 0.5% bovine serum albumin (BSA). Finally, the slices were incubated overnight at 4°C with streptavidin-conjugated Alexa-546 (dilution, 1:200; Jackson ImmunoResearch Laboratories, Inc., West Grove, PA, USA, Baltimore Pike, PA, USA) in TBS containing 1% NGS and 0.5% BSA. The following day, sections were rinsed with TBS and mounted in Dako fluorescence medium (Dako Canada Inc., Mississauga, ON, Canada). Confocal images of biocytin-filled INs were obtained using a Leica TCS SP5 imaging system coupled with a 543 nm He–Ne laser. IN Z-stacks were acquired with a 1 μm step. Final stacks containing different parts of INs were merged in Neurolucida 8.26.2 (Williston, VT, USA) and selected cells were reconstructed.

For immunocytochemical analysis, whole-cell recordings were performed for a maximum of 5 min, during which neurons were filled with fluorescein dextran (0.2%; Invitrogen). Slices with recorded neurons were fixed with 4% paraformaldehyde, embedded in 2% agar and re-sectioned to 40 μm. Sections were treated with hydrogen peroxide, permeabilized with 0.2% Triton X-100 in TBS containing normal donkey serum (1%) and BSA (2%) and incubated overnight at 4°C with a rabbit cholecystokinin antibody (dilution, 1:6000; Sigma-Aldrich, St Louis, MO, USA). The following day, sections were rinsed with TBS and incubated with an anti-rabbit Texas Red secondary antibody (dilution, 1:200; Jackson ImmunoResearch) for 1.5 h. Sections were then rinsed in TBS and mounted in Dako fluorescence medium (Dako Canada Inc.). Images were captured using a Leica TCS SP5 system.

Chemicals

In some experiments, one of the following drugs was added to the ACSF: the L-type VSCC blocker nifedipine (10 μM), the R-type VSCC antagonist SNX-482 (30 nM), the selective T-type VSCC blocker NNC 55-0396 (10 μM), the P/Q-type VSCC antagonist ω-agatoxin IVA (AgTx, 250 nM), the N-type VSCC antagonist ω-conotoxin GVIA (CTx, 250 nM) or the SERCA inhibitor cyclopiazonic acid (CPA, 30 μM). A combination of all VSCC blockers and of CPA (cocktail; Fig. 4*C*) or of DL-AP5 (50 μM) and NBQX (10 μM) were applied when indicated. All chemicals were stored as stock solutions at −20°C, diluted on the day of the experiment and either added to the perfusion system (nifedipine, NNC 55-0396, CPA, DL-AP5 and NBQX) or applied directly into the recording chamber (toxins). In some experiments, BAPTA (10 mM) was included in the patch solution (Fig. 8*B* and *C*). Nifedipine, SNX-482, NNC 55-0396, CPA and BAPTA were purchased from Sigma, and ω-agatoxin IVA and ω-conotoxin GVIA were obtained from Alomone Labs (Jerusalem, Israel). DL-AP5 and NBQX were obtained from Ascent Scientific (Princeton, NJ, USA).

Results

Identification of INs based on anatomical, neurochemical and electrophysiological criteria

In the present study, a total of 274 INs were recorded in the CA1 stratum radiatum (RAD). Of these cells, 223 neurons

were labelled successfully with biocytin and reconstructed anatomically. Based on anatomical criteria, 72 recorded neurons were identified as basket cells (BCs), and 69 neurons were identified as Schaffer collateral-associated cells (SC-ACs; Fig. 1*A*). In particular, both cell types had extensive dendritic branching in the RAD, stratum pyramidale (PYR) and oriens/alveus (O/A), but were clearly distinguishable based on their axonal arborizations. The axons of SC-ACs ran almost entirely (∼90%) within the RAD, with a few branches entering the PYR and O/A (Fig. 1*Aa*, 3*Da*, 4*Da*, 5*C*, 6*Da*, 7*E* and 8*Da*). In contrast, the axons of BCs covered essentially the PYR and the adjacent part of the O/A and RAD, largely following the orientation of the pyramidal layer (Fig. 1*Ab*, 3*Db*, 4*Db*, 5*D*, 6*Db*, 7*F* and 8*Db*). INs that were identified anatomically were then compared in terms of their electrophysiological

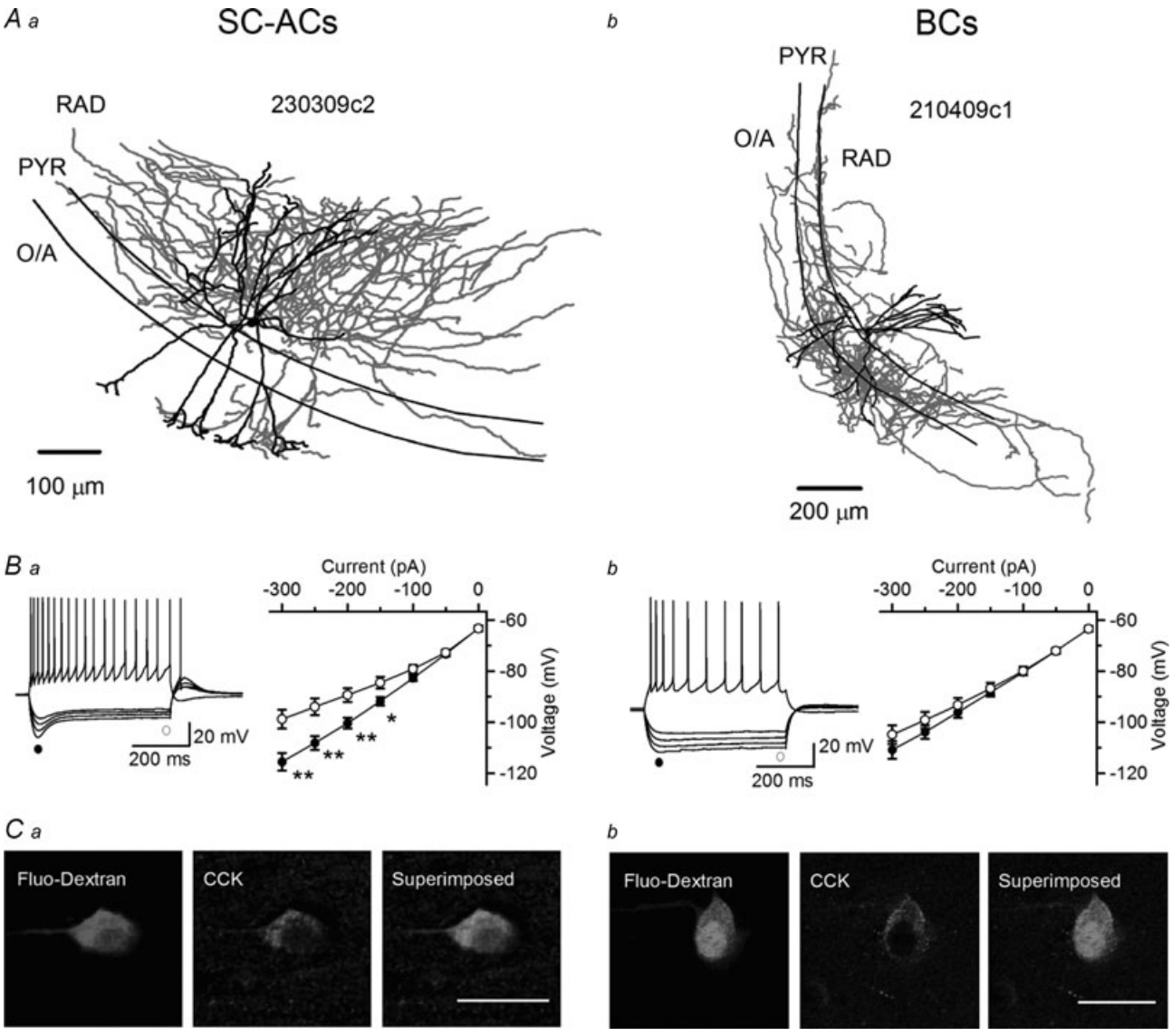

Figure 1. Comparison of the anatomical, electrophysiological and neurochemical properties of hippocampal CA1 basket cells and Schaffer collateral-associated cells
A, Neurolucida reconstructions of biocytin-filled INs with axonal (red) and dendritic (black) arborizations in different layers. *B*, voltage responses of an SC-AC (*Ba*) and a BC (*Bb*) to hyperpolarizing and depolarizing current injections (left) and current–voltage plots of peak (●) and steady-state (○) voltage responses to hyperpolarizing currents (right). Both SC-ACs and BCs showed a regularly spiking firing pattern, whereas only SC-ACs exhibited a significant response rectification (I_h) evoked by membrane hyperpolarization and a rebound spike. $^*P < 0.05$, $^{**}P < 0.01$, paired *t* test. *C*, confocal images showing immunoreactivity for cholecystokinin (CCK; middle) in putative SC-ACs (*Ca*) and BCs (*Cb*) that were filled with fluorescein dextran during recordings (left) and were identified based on the similarity of their electrophysiological properties to those of anatomically reconstructed INs. Scale bars, 20 μm.

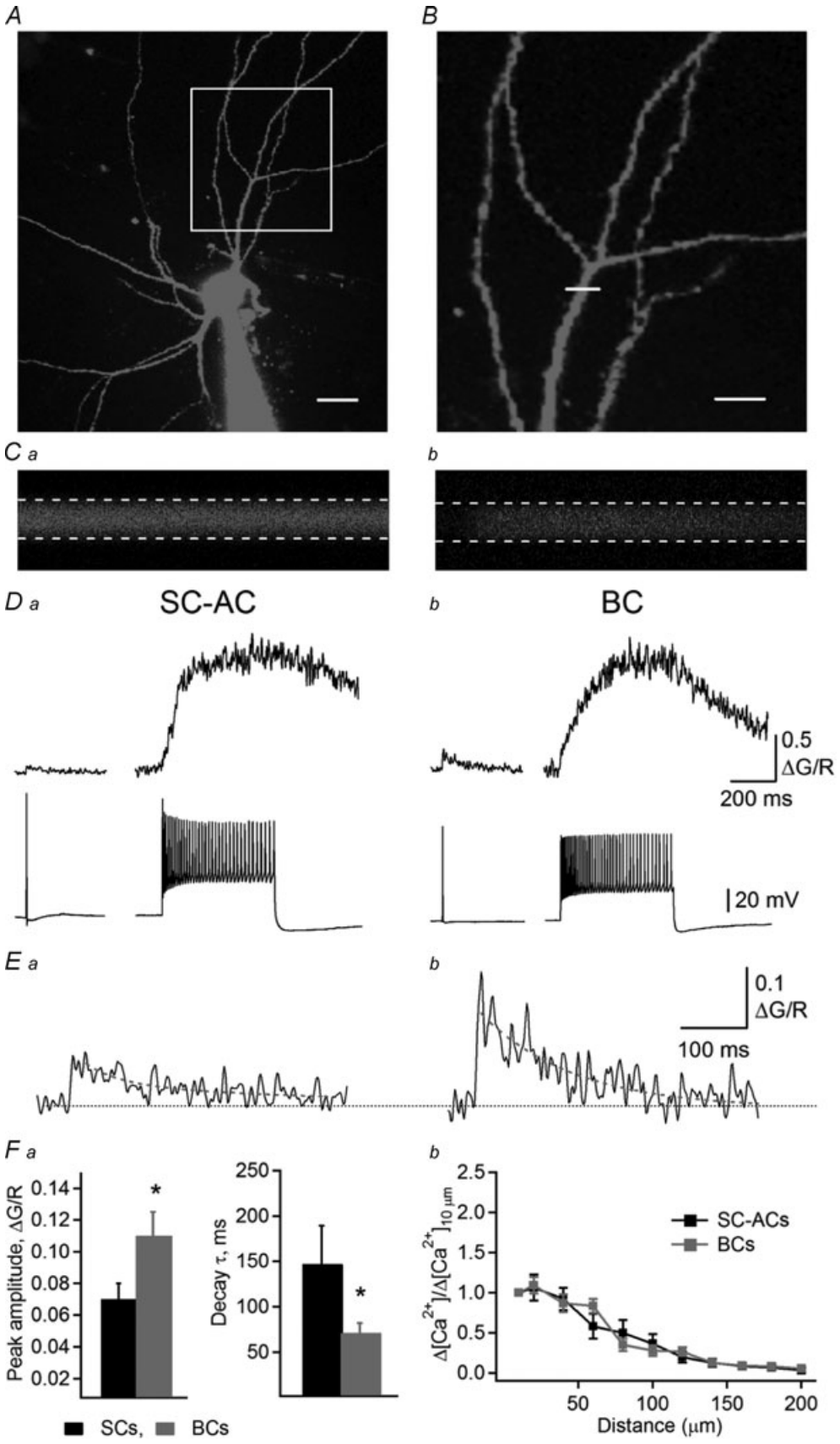

properties (Fig. 1*B*). Consistent with previous findings (Vida *et al.* 1998; Cope *et al.* 2002; Pawelzik *et al.* 2002), both cell types exhibited a regularly spiking firing pattern but differed in their response to hyperpolarizing current injections, with SC-ACs showing a significant hyperpolarization-activated I_h current and a rebound depolarizing potential followed by a spike (Fig. 1*Ba*) and the BCs demonstrating a small or no I_h and lacking the rebound spike (Fig. 1*Bb*). Finally, in a separate series of experiments, INs were recorded for 5 min, during which electrophysiological properties were determined and cells were filled with fluorescein dextran to allow *post hoc* neurochemical identification (Fig. 1*C*). Twelve recorded neurons proved to be cholecystokinin-immunoreactive (CCK-IR) neurons, of which five were regularly spiking neurons with a large I_h and a rebound spike (properties typical of SC-ACs; Fig. 1*Ba* and 1*Ca*), and seven were regularly spiking cells lacking I_h and a rebound spike (features of BCs; Fig. 1*Bb* and 1*Cb*). Therefore, these cells were considered as CCK-positive SC-ACs and BCs, based on the expression of CCK and the similarity of their electrophysiological properties to those of SC-ACs and BCs identified anatomically and recorded in Ca^{2+} imaging experiments. Given that a typical Ca^{2+} imaging experiment required at least 60 min of whole-cell recording followed by extensive wash-out of intracellular content (Pusch & Neher, 1988; Müller *et al.* 2005), we were not able to identify neurochemically INs filled with biocytin during Ca^{2+} imaging experiments. Accordingly, for the remainder of this study, we based the identification of INs exclusively on a combination of anatomical and electrophysiological criteria. All recorded regularly spiking INs were divided into two groups: SC-ACs if they had ∼90% of axonal arborization within the RAD and a prominent I_h and a rebound spike, and BCs if they had axons ramifying within the PYR with electrophysiological properties typical for BCs (lacking I_h and the rebound spike). Accordingly, cells that showed different morphologies (axons ramifying in all layers or directed to the stratum lacunosum-moleculare; densely packed axons) or electrophysiological properties (fast-spiking, rapidly adapting or irregularly spiking stuttering firing pattern) were excluded from the analysis ($n = 82$).

Larger and faster Ca^{2+} transients in dendrites of BCs

Combined two-photon Ca^{2+} imaging and patch-clamp whole-cell recordings were performed in RAD INs at a temperature of 30–32°C. INs were filled with a combination of green medium-affinity Ca^{2+} indicator (Fluo-5F) and a Ca^{2+}-insensitive red fluorophore (Alexa-594; to assess dendritic morphology, Fig. 2*A*–*C*). After the dye-loading period (20–30 min), INs were held in the current clamp mode and short depolarizing pulses (0.8–1 nA, 2 ms) were used to trigger an AP. AP-CaTs were measured in proximal dendritic branches up to 200 μm from the soma (Fig. 2). The dendritic diameter in this region was similar in both cell types (BCs, 3.7 ± 0.1 μm, $n = 9$; SC-ACs, 3.5 ± 0.1 μm, $n = 8$; $P > 0.05$). However, in BCs, AP-CaTs that were evoked by single APs had a large amplitude ($\Delta G/R$: 0.11 ± 0.02, $n = 11$) and a relatively fast decay time constant (70.7 ± 11 ms, $n = 9$; Fig. 2*D*, *E* and *Fa*). In contrast, in SC-ACs, AP-CaTs exhibited a significantly smaller amplitude ($\Delta G/R$: 0.07 ± 0.01, $n = 9$, $P < 0.05$) and slower decay kinetics (147 ± 42.1 ms, $n = 8$, $P < 0.05$; Fig. 2*D*, *E* and *Fa*). In both cell types, AP-CaTs were completely abolished by tetrodotoxin (1 μM), indicating that they were mediated by back-propagating APs.

To determine the actual amplitude of Ca^{2+} rises in IN dendrites and to compare it between different cell types, we converted $\Delta G/R$ to Ca^{2+} concentration ($[Ca^{2+}]_{AP}$) using a method developed by the group of Svoboda (Maravall *et al.* 2000; Sabatini *et al.* 2002; Yasuda *et al.* 2004), which relies on the determination of the fluorescence of the Ca^{2+} indicator at saturating $[Ca^{2+}]$ ($\Delta G/R_{max}$) (eqn (2); Fig. 2*D*). The value of $\Delta G/R_{max}$ was obtained from the plateau fluorescence reached during AP trains at 60–80 Hz (Fig. 2*D*). On average, $[Ca^{2+}]_{1AP}$ was significantly larger in BCs compared with SC-ACs (BCs: 212 ± 34 nM, $n = 11$ *vs.* SC-ACs: 131 ± 15 nM, $n = 9$; $P < 0.05$). In both cell types, $[Ca^{2+}]_{APs}$ declined significantly at distances from the cell body exceeding 60 μm and were almost undetectable in distal dendrites (>150 μm; Fig. 2*Fb*).

Given that the presence of exogenous Ca^{2+} buffer perturbs the dynamics of Ca^{2+} signals significantly (Helmchen *et al.* 1996), we next inferred $[Ca^{2+}]_{AP}$

Figure 2. Imaging dynamics of action potential-evoked Ca^{2+} transients in IN dendrites
A, two-photon image (maximum projection of a Z-stack) of an IN filled with Alexa-594 and Fluo-5F. Scale bar, 20 μm. *B*, magnified image of a dendritic arbour (boxed region in *A*). The white line across the dendrite indicates the position of the linescan. Scale bar, 20 μm. *C*, linescan images obtained from the red (*Ca*) and green (*Cb*) channels simultaneously, in response to an 80 Hz train of backpropagating APs. Dashed lines indicate the region of interest for signal measurements. *D*, representative CaTs evoked by a single AP (left) or by saturating trains (right) in SC-ACs (*Da*) and BCs (*Db*). *E*, expanded traces of CaTs evoked by a single AP in SC-ACs (*Ea*) and BCs (*Eb*). Red lines correspond to double exponential fits. *F*, summary data showing the differences in the CaT peak amplitude (*Fa*, left) and decay time constant (*Fa*, right), as well as $[Ca^{2+}]$ changes as a function of distance (*Fb*) in the two cell types. Data for SC-ACs are shown in black and data for BCs are shown in red.

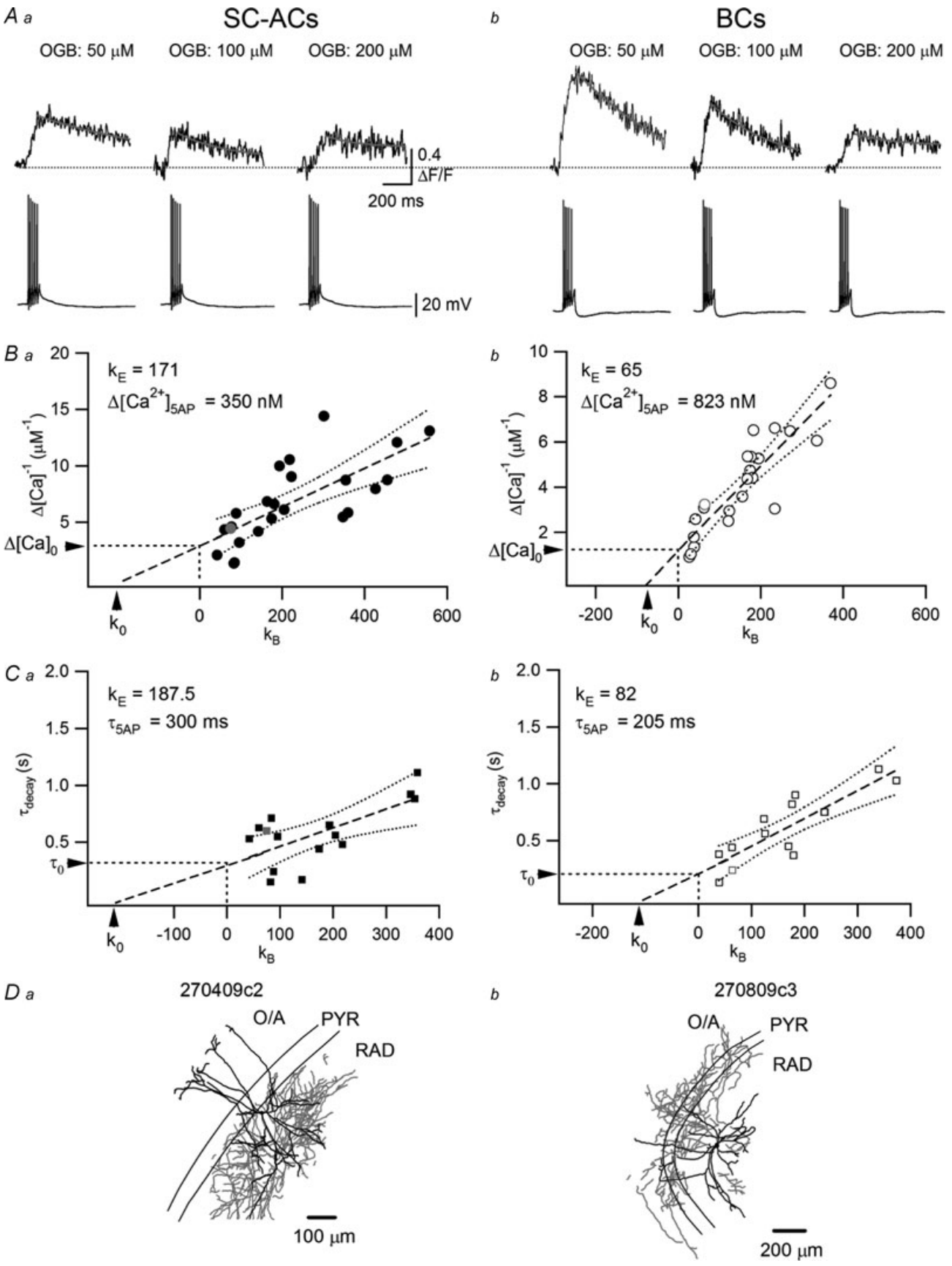

dynamics in the absence of the indicator. For this series of experiments, cells were loaded with various concentrations of a bright, high-affinity Ca^{2+} indicator (Oregon Green BAPTA-1: 50, 100 and 200 μM; Fig. 3) and AP-CaTs were evoked by small bursts of five APs (to obtain clearly defined fluorescence transients that allow precise measurements of the decay kinetics at different dye concentrations). Resting Ca^{2+} concentrations ($[Ca^{2+}]_0$), $\Delta[Ca^{2+}]_{5APs}$ and τ_{decay} were determined for each indicator concentration. $[Ca^{2+}]_0$ was similar in both cell types (BCs: 64 ± 5 nM, $n = 22$; SC-ACs: 60 ± 4 nM, $n = 23$; $P > 0.05$; eqn (3)) and did not vary significantly with the concentration of the indicator (50 μM OGB-1, 77 ± 8 nM, $n = 13$; 100 μM OGB-1, 60 ± 7 nM, $n = 21$; 200 μM OGB-1, 77 ± 13 nM, $n = 11$; $P > 0.05$; ANOVA). As expected, $\Delta[Ca^{2+}]_{5APs}$ decreased and τ_{decay} increased linearly as a function of indicator concentration and, accordingly, total buffer capacity (Fig. 3*A*). Extrapolation to 'zero' buffer concentration (the *y*-axis intercept of the linear fits to the data points) allowed the determination of $\Delta[Ca^{2+}]_{5APs}$ and τ_{decay} under native conditions (without added Ca^{2+} buffer). Accordingly, in dendrites of BCs, $\Delta[Ca^{2+}]_{5AP}$ values were of larger amplitude and faster kinetics ($\Delta[Ca^{2+}]_{5APs}$: 0.82 μM (0.5–2.8 μM); τ_{decay}: 205 ms (30–388 ms)) compared with those recorded in dendrites of SC-ACs ($\Delta[Ca^{2+}]_{5APs}$: 0.35 μM (0.21–1.0 μM); τ_{decay}: 300 ms (85–515 ms), Fig. 3*B* and *C*).

To determine whether the differences in the amplitude and kinetics of Ca^{2+} rises between the two cell types arose from different endogenous Ca^{2+} buffering capacities in their dendrites, the endogenous binding capacity in the absence of added Ca^{2+} buffers (κ_S) was derived from the *x*-axis intercepts of the fits (κ_0; Fig. 3*B*, *C*). From the $1/\Delta[Ca^{2+}]_{5APs}$ *vs.* κ_B relationship, κ_S was found to be lower in the dendrites of BCs compared with those of SC-ACs (BCs: 65 (28–88); SC-ACs: 171 (100–201); Fig. 3*B*). Similarly, from the τ_{decay} *vs.* κ_B relationship, κ_S was found to be lower in the dendrites of BCs (BCs: 82 (14–114); SC-ACs: 187 (152–189); Fig. 3*C*). These results suggest that the significantly larger amplitude and faster decay kinetics observed for AP-evoked Ca^{2+} rises in the dendrites of BCs compared with those of SC-ACs can arise from differences in the endogenous Ca^{2+} binding capacities between these cells.

Action potential-evoked dendritic Ca^{2+} transients were regulated actively by changes in IN activity

According to the results presented so far, dendritic Ca^{2+} transients evoked by backpropagating APs in two types of hippocampal INs differ significantly due to the cell type-specific properties of Ca^{2+} handling, in particular to endogenous Ca^{2+} buffering capacities. To examine whether these quantitatively different CaTs may also involve distinct Ca^{2+} mechanisms, next we assessed their sensitivity to specific blockers of VSCCs and of intracellular Ca^{2+} stores (Fig. 4). Experiments were performed using Fluo-5F as a Ca^{2+} indicator. The L-type VSCC blocker nifedipine (10 μM; Fig. 4*Aa*, *Ba* and *C*) decreased the AP-CaT amplitude to ~70% of that of the control in both cell types, indicating a significant contribution of L-type VSCCs to dendritic AP-CaTs in SC-ACs and BCs. However, the effects of the T-type VSCC blocker NNC 55-0396 (10 μM; Fig. 4*Ab*, *Bb* and *C*), which is a modified mibefradil analogue that is exquisitely selective for T-type VSCCs when used at low concentration (Huang *et al.* 2004; Li *et al.* 2005), and of the P/Q-type VSCC blocker ω-agatoxin IVA (AgTx, 250 nM; Fig. 4*Ac*, *Bc* and *C*) were cell type specific. T-type VSCCs exhibited a significantly higher contribution in the dendrites of SC-ACs (SC-ACs, 39.6 ± 4.1% of AP-CaTs, $n = 5$; BCs, 20.5 ± 5.7% of AP-CaTs, $n = 6$; $P < 0.05$, unpaired *t* test), whereas P/Q-type VSCCs were recruited by APs only in the dendrites of BCs (SC-ACs, 2.5 ± 0.2% of AP-CaTs, $n = 6$; BCs, 28.2 ± 3.4% of AP-CaTs, $n = 6$; Fig. 4*C*). Furthermore, the inhibitors of R-type (SNX-482, 30 nM) and N-type (CTx, 250 nM) VSCCs had no effect in either cell type (Fig. 4*Aa*, *Ba*, *Ac*, *Bc* and *C*), suggesting that these channels do not contribute to dendritic AP-CaTs in SC-ACs and BCs. In addition, both cell types demonstrated a significant component mediated by the activation of intracellular Ca^{2+} stores (Fig. 4*Ab*, *Bb* and *C*), pointing to the Ca^{2+}-induced Ca^{2+} release activated in IN dendrites by backpropagating APs.

Figure 3. Estimation of $[Ca^{2+}]_{AP}$ dynamics and endogenous buffer capacity
A, representative CaTs (top) recorded with different concentrations of OGB-1 in response to five APs (bottom) in SC-ACs (*Aa*) and BCs (*Ab*). *B*, summary plots of the inverse of the peak amplitude of AP-CaTs ($1/\Delta[Ca^{2+}]_{5APs}$), as a function of added Ca^{2+} buffer capacity (κ_B) for SC-ACs (*Ba*) and BCs (*Bb*). The intercepts of linear fits (straight dashed lines) with the *x*-axis were used to estimate the endogenous Ca^{2+} binding capacity (κ_0), whereas the fit extrapolation to 'zero' buffering conditions was used to derive the amplitude of $[Ca^{2+}]_{5APs}$ in the absence of dye ($\Delta[Ca^{2+}]_0$). *C*, summary plots of the decay time constant as a function of added Ca^{2+} buffer capacity (κ_B) for SC-ACs (*Ca*) and BCs (*Cb*). Arrows indicate the calculated endogenous Ca^{2+} binding capacity (κ_0) and τ_{decay} in the absence of added buffer (τ_0). Dashed lines are the best linear fits to the data and the dotted lines are the 95% confidence bands of the fits. *D*, Neurolucida reconstructions of two representative biocytin-filled INs with axonal (red) and dendritic (black) arborizations in different layers.

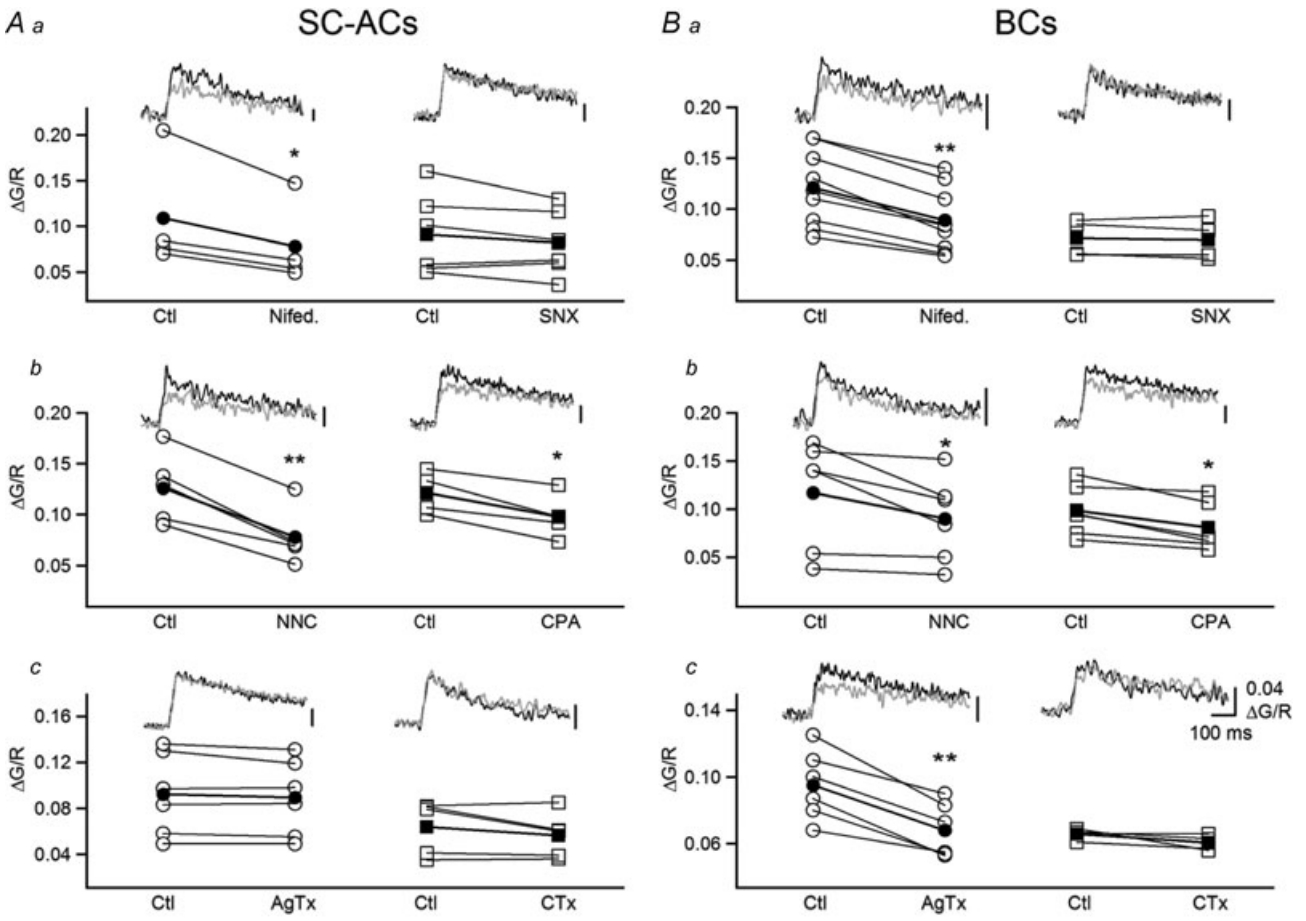

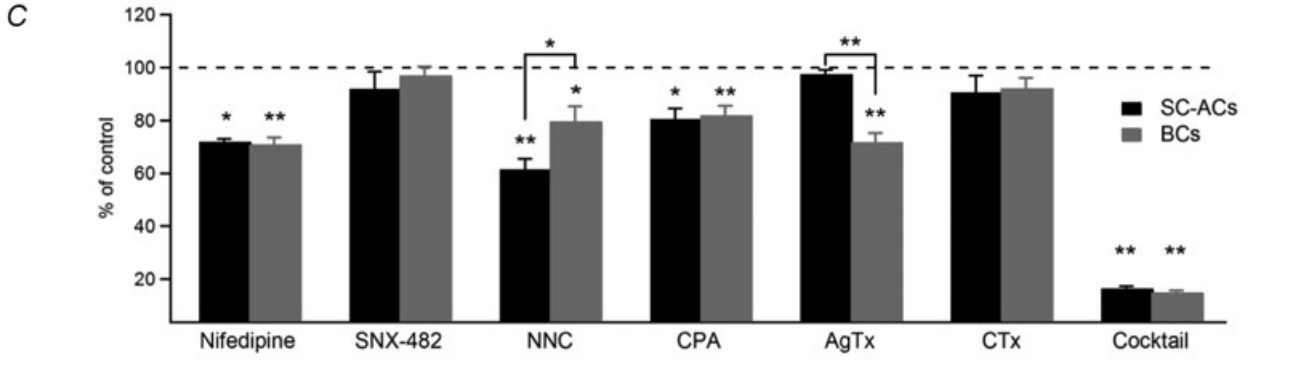

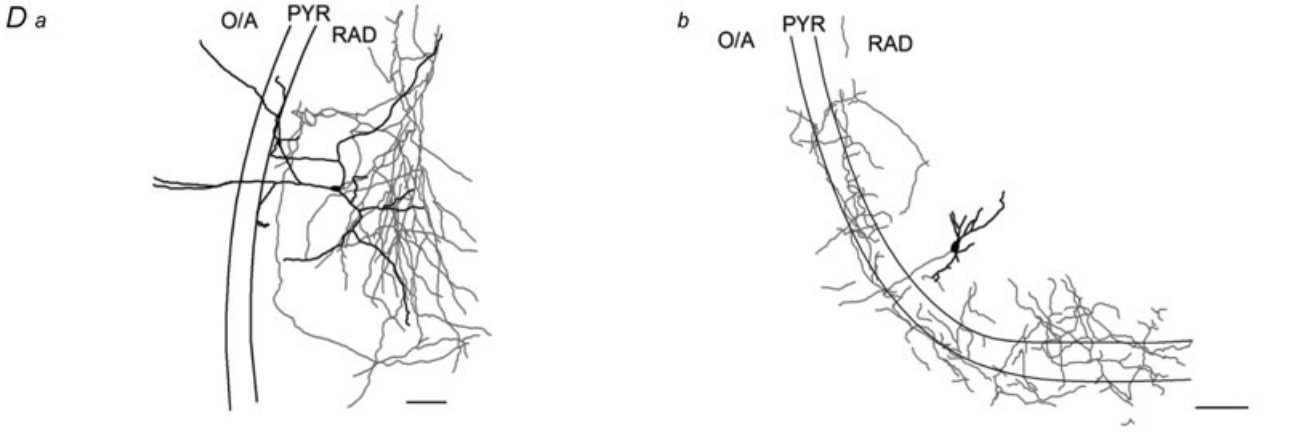

During theta rhythm *in vivo*, most hippocampal INs go through active and relatively silent states (Klausberger *et al.* 2003) during which the IN membrane potential should fluctuate from a relatively depolarized to a hyperpolarized level, respectively. Given a cell type-specific contribution of VSCCs in the IN dendrites, we examined next whether AP-CaTs can be differentially affected by the membrane potential fluctuations in two types of INs. In SC-ACs, the transition from −60 to −80 mV significantly increased the amplitude of dendritic Ca^{2+} rises (to 137 ± 7% of the control, $n = 5$, $P < 0.001$; Fig. 5*Aa* and *B*). This increase in $\Delta[Ca^{2+}]_{APs}$ at −80 mV was not affected by the L-type VSCC blocker nifedipine (10 μM; $n = 4$; Fig. 5*Aa* and *B*) but was prevented in the presence of the more specific T-type VSCC blocker NNC 55-0396 (Huang *et al.* 2004) used at low concentration here (10 μM; $n = 4$; Fig. 5*Aa* and *B*), which suggests that the hyperpolarization-induced enhancement of $\Delta[Ca^{2+}]_{APs}$ in the dendrites of SC-ACs is mediated by enhanced recruitment of T-type VSCCs. In contrast, in dendrites of BCs, the transition from −60 to −80 mV was associated with a significant decrease in the amplitude of Ca^{2+} rises (to 84 ± 3% of the control, $n = 6$, $P < 0.05$; Fig. 5*Ab* and *B*), which was not affected by NNC 55-0396 ($n = 5$) but was prevented by nifedipine ($n = 5$; Fig. 5*Ab* and *B*). These results indicate that, for any phase of the theta wave, IN dendritic $\Delta[Ca^{2+}]_{APs}$ will fluctuate in a cell type-specific manner, which is determined by the cell type-specific contribution of distinct types of VSCCs to IN dendritic Ca^{2+} signalling.

In vivo, many INs fire spikes during the gamma-rhythm episodes (40–100 Hz) associated with exploratory walking and paradoxical sleep (Soltesz & Deschênes, 1993; Bragin *et al.* 1995). Gamma-like firing episodes (63 Hz) affect the state of dendritic VSCCs profoundly in pyramidal cells, interfering with the induction of long-term synaptic plasticity (Yasuda *et al.* 2003). However, whether brief episodes of high-frequency firing have an effect on AP-evoked Ca^{2+} dynamics in dendrites of INs remains unexplored, and was tested here. As shown in Fig. 6*Aa*, brief trains of high-frequency firing (60–80 Hz, 0.5 s, repeated 2–3 times) did not affect AP-CaTs in the dendrites of SC-ACs ($P > 0.05$, $n = 4$; Fig. 6*Aa*, *Ba* and *Ca*). In contrast, the amplitude of dendritic AP-CaTs was significantly decreased in the dendrites of BCs (to 64 ± 5% of control, $n = 6$, $P < 0.05$; Fig. 6*Ab*, *Bb* and *Cb*). This depression was blocked by nifedipine ($n = 4$; Fig. 6*Bb* and *Cb*), which suggests that it required the activation of L-type VSCCs. These data indicate that AP-evoked dendritic Ca^{2+} rises are differentially regulated in different types of INs that exhibit the same activity patterns. Therefore, in addition to the cell type-specific properties of dendritic Ca^{2+} handling, Ca^{2+} transients may undergo specific forms of plasticity that are likely to be controlled by the cell type-specific expression and/or availability of particular ion channels, signalling molecules and/or downstream cascades.

Summation of Ca^{2+} transients during theta bursting and its role in synaptic plasticity

It has been demonstrated that during hippocampal theta-rhythm activity *in vivo* (3–12 Hz), most of the inhibitory INs fire two to three APs (at 100 Hz) coupled in a cell type-specific manner to different phases of the theta oscillation (Klausberger *et al.* 2003; Klausberger, 2009). According to our findings so far, such common theta-burst firing (TBF) of different classes of hippocampal INs should be translated into cell type-specific Ca^{2+} signalling in their dendrites, which may play an important role in the induction of synaptic plasticity (Perez *et al.* 2001; Patenaude *et al.* 2005). This assumption was tested in the next series of experiments (Fig. 7). Experiments were performed using Fluo-5F as a Ca^{2+} indicator. Three APs at 100 Hz frequency were evoked by brief current injections (0.8–1 nA, 2 ms) and repeated 2 to 5 times (2–5 bursts) with a rate of 4 Hz. It was apparent that $\Delta[Ca^{2+}]_{3APs}$ evoked by individual bursts of three APs in dendrites of BCs were significantly larger than those evoked in SC-ACs (BCs: 0.63 ± 0.14 μM, $n = 6$ *vs.* SC-ACs: 0.38 ± 0.11 μM, $n = 4$; $P < 0.05$; Fig. 7*A* and *B*). Considering the amplitude of Ca^{2+} rises evoked by individual APs (BCs: 0.21 ± 0.03 nM, $n = 11$ *vs.* SC-ACs: 0.131 ± 0.015 nM, $n = 9$), this corresponds to a linear summation of Ca^{2+} transients during three APs at 100 Hz in both cell types (Fig. 7*C*). However,

Figure 4. Differential contribution of voltage-sensitive Ca^{2+} channels to action potential-evoked Ca^{2+} transients in IN dendrites
A and *B*, summary plots and representative AP-CaTs recorded using Fluo-5F in a control setting (black trace) and 10–15 min after the administration of blockers (green trace) of L-type (nifedipine, 10 μM; *Aa*, *Ba*, left), R-type (SNX-482, 10 μM; *Aa*, *Ba*, right), T-type (NNC 55-0396, 10 μM; *Ab*, *Bb*, left), P/Q-type (ω-agatoxin IVA (AgTx), 250 nM; *Ac*, *Bc*, left) and N-type (ω-conotoxin GVIA (CTx), 250 nM; *Ac*, *Bc*, right) VSCCs and intracellular Ca^{2+} stores (CPA, 30 μM; *Ab*, *Bb*, right) in SC-ACs (*A*) and BCs (*B*). *C*, summary bar graph of group data for AP-CaT mechanisms, showing that L- and T-type VSCCs and stores contributed to AP-CaTs in SC-ACs, whereas L-, T- and P/Q-type VSCCs and stores mediated AP-CaTs in BCs. Data are expressed as percentages of control CaTs obtained prior to drug application. *D*, Neurolucida reconstructions of the two representative biocytin-filled INs from which the recordings were obtained, with axonal arborization shown in red and dendrites shown in black.

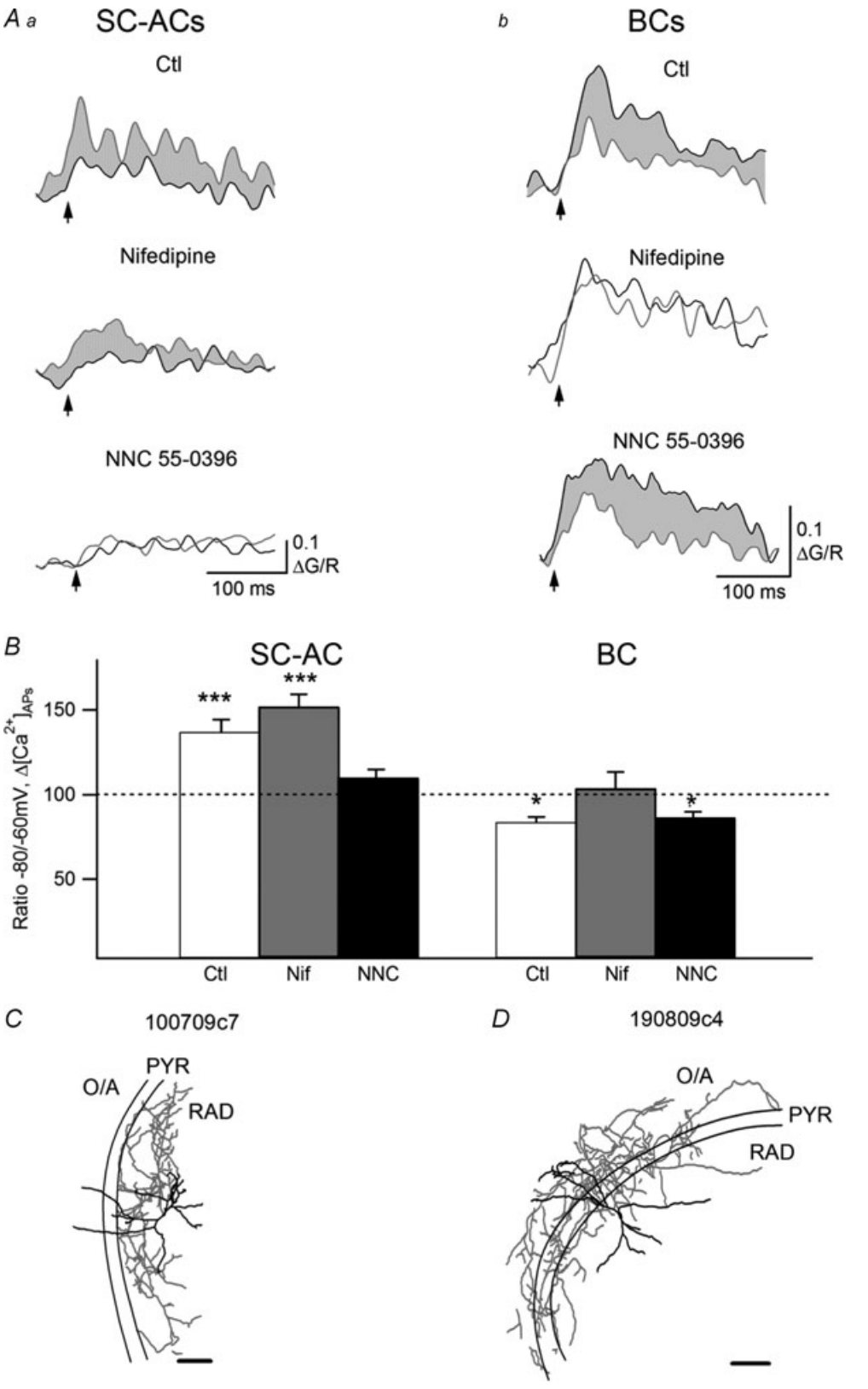

Figure 5. Regulation of action potential-evoked Ca^{2+} transients by membrane potential
A, representative examples of AP-CaTs (average of three) evoked in SC-ACs (*Aa*) and BCs (*Ab*) by a burst of three APs applied at −60 mV (black) and at −80 mV (red) in control (top) and in the presence of the L-type VSCC blocker nifedipine (10 μM, middle) or the T-type VSCC blocker NNC 55-0396 (10 μM, bottom) tested in different

during TBF, the summation degree of Ca^{2+} transients appeared to be larger for SC-ACs (Fig. 7*C*), and reached a significantly higher level than in BCs at the fifth burst (BCs: $\Delta[Ca^{2+}]_{5bursts} = 5.65 \pm 0.93$ of $\Delta[Ca^{2+}]_{1AP}$, $n = 6$ *vs.* SC-ACs: $\Delta[Ca^{2+}]_{5bursts} = 9.22 \pm 0.94$ of $\Delta[Ca^{2+}]_{1AP}$, $n = 4$, $P < 0.05$; Fig. 7*C*). Thus, even though the amplitude of Ca^{2+} rises evoked by individual bursts was smaller in SC-ACs, the peak amplitude of SC-ACs' $\Delta[Ca^{2+}]_{APs}$ was able to reach the BCs' level by the fifth burst due to a more efficient temporal summation (Fig. 7*A*). Since the previous findings of this study indicate that SC-ACs' Ca^{2+} rises demonstrate slower decay kinetics compared with BCs, largely due to the differences in the endogenous Ca^{2+} binding capacities between the two cell types (Figs 2 and 3), these results suggest that the enhanced temporal summation of $\Delta[Ca^{2+}]_{APs}$ during TBF in SC-ACs could result from slowing in their $\Delta[Ca^{2+}]_{APs}$ decays. The plot in Fig. 7*D* shows a more prominent increase in the τ_{decay} in dendrites of SC-ACs during TBF compared with that in BCs, and a significant difference in the decay kinetics of $\Delta[Ca^{2+}]_{APs}$ between the two cell types. Thus, the slowing of Ca^{2+} transient decay kinetics in SC-ACs enhanced the temporal summation of their Ca^{2+} signals in such a way that initially small Ca^{2+} signals became equal to those in BCs during TBF.

Theta-burst firing has been associated with the induction of Ca^{2+}-dependent forms of synaptic plasticity at both excitatory and inhibitory synapses (Perez *et al.* 2001; Patenaude *et al.* 2005). In most cases, theta-burst-induced plasticity requires the pairing of post-synaptic firing with presynaptic stimulation. However, it remains unclear whether TBF alone, which is associated with the activation of multiple types of VSCCs and a massive Ca^{2+} influx in IN dendrites, is sufficient to support the induction of synaptic plasticity. Spatial restriction of AP-CaTs to proximal dendritic sites (Fig. 2*F*), together with a similar spatial distribution of inhibitory synapses onto RAD INs (Gulyas *et al.* 1999; Pettit & Augustine, 2000), suggests that inhibitory transmission to INs is in particular controlled by these Ca^{2+} signals. To test this hypothesis, next we examined whether TBF alone was sufficient to induce long-term plasticity at inhibitory synapses onto both SC-ACs and BCs. Monosynaptic IPSCs in INs held at −50 mV were evoked by local stimulation in the RAD in the presence of DL-AP5 and NBQX. In control recordings, IPSC amplitude remained stable for at least 30 min (100.9 ± 1.0% of the response recorded during the first 5 min, $n = 8$; $P > 0.05$). In contrast, long-term potentiation (LTP) of IPSCs (163.1 ± 4.9% of the control, $n = 7$; $P < 0.05$; Fig. 8*B*) was observed after TBF (2 s each, repeated three times at 30 s intervals) and was independent of cell type. Importantly, no significant difference was observed in the magnitude of IPSC potentiation between the two cell types (BC-LTP, 170.6 ± 4.9% of the control, $n = 4$; SC-AC-LTP, 153.1 ± 5.3% of the control, $n = 3$; $P > 0.05$; Fig. 8*A*), which suggests the presence of a similar mechanism of LTP induction at inhibitory synapses onto both SC-ACs and BCs. Accordingly, LTP was expressed presynaptically in both cell types, as it was associated with a significant decrease in the PPR (71.8 ± 4.5% of the control, $n = 7$; $P < 0.05$; Fig. 8*C*) and CV (89.3 ± 3.3% of the control, $n = 7$; $P < 0.05$; Fig. 8*C*). Moreover, in both cell types, this presynaptic LTP required the elevation of postsynaptic Ca^{2+}, as it was blocked when BAPTA was included in the patch solution (98.7 ± 1.3% of the control, $n = 4$; $P > 0.05$; Fig. 8*B* and *C*). Together, these data indicate that significant Ca^{2+} elevations, which result from the efficient summation of AP-CaTs during TBF in both BCs and SC-ACs, control the induction of a pre-synaptic form of LTP at inhibitory synapses onto these cells.

Discussion

Cell type-specific properties of action potential-evoked dendritic Ca^{2+} transients in INs

Experimental approaches based on combined two-photon dendritic Ca^{2+} imaging and patch-clamp recordings from rigorously identified inhibitory INs are important for the clarification of the role played by cell type-specific dendritic integration in the function of INs. The majority of inhibitory INs show high endogenous Ca^{2+} binding capacities and, as a result, small amplitudes and slow kinetics of dendritic Ca^{2+} transients (Lee *et al.* 2000; Kaiser *et al.* 2001; Aponte *et al.* 2008). INs are also endowed with a large repertoire of active dendritic conductances (Martina *et al.* 2000; Goldberg *et al.* 2003; Vinet & Sík, 2006; Hu *et al.* 2010), specific signalling molecules and cascades (Liu & Jones, 1996; Sík *et al.* 1998; Topolnik *et al.* 2006) in a cell type-specific manner and are, thus, predisposed to distinct forms of activity-dependent regulation and network behaviour. The mechanisms of activity-dependent regulation of IN dendritic signalling

experiments. Red shadowed areas show increases in CaTs in SC-ACs whereas grey shadowed areas correspond to AP-CaTs' decreases in BCs. *B*, summary bar graph showing the ratio of the amplitudes of $\Delta[Ca^{2+}]_{3APs}$ at −80 and −60 mV, which were measured in control conditions and in the presence of nifedipine (Nif) and NNC 55-0396 (NNC). $^{*}P < 0.05$, $^{***}P < 0.001$, paired *t* test. Data were recorded using Fluo-5F as a Ca^{2+} indicator. *C* and *D*, Neurolucida reconstructions of two representative INs from which the recordings were obtained. Scale bars, 200 μm.

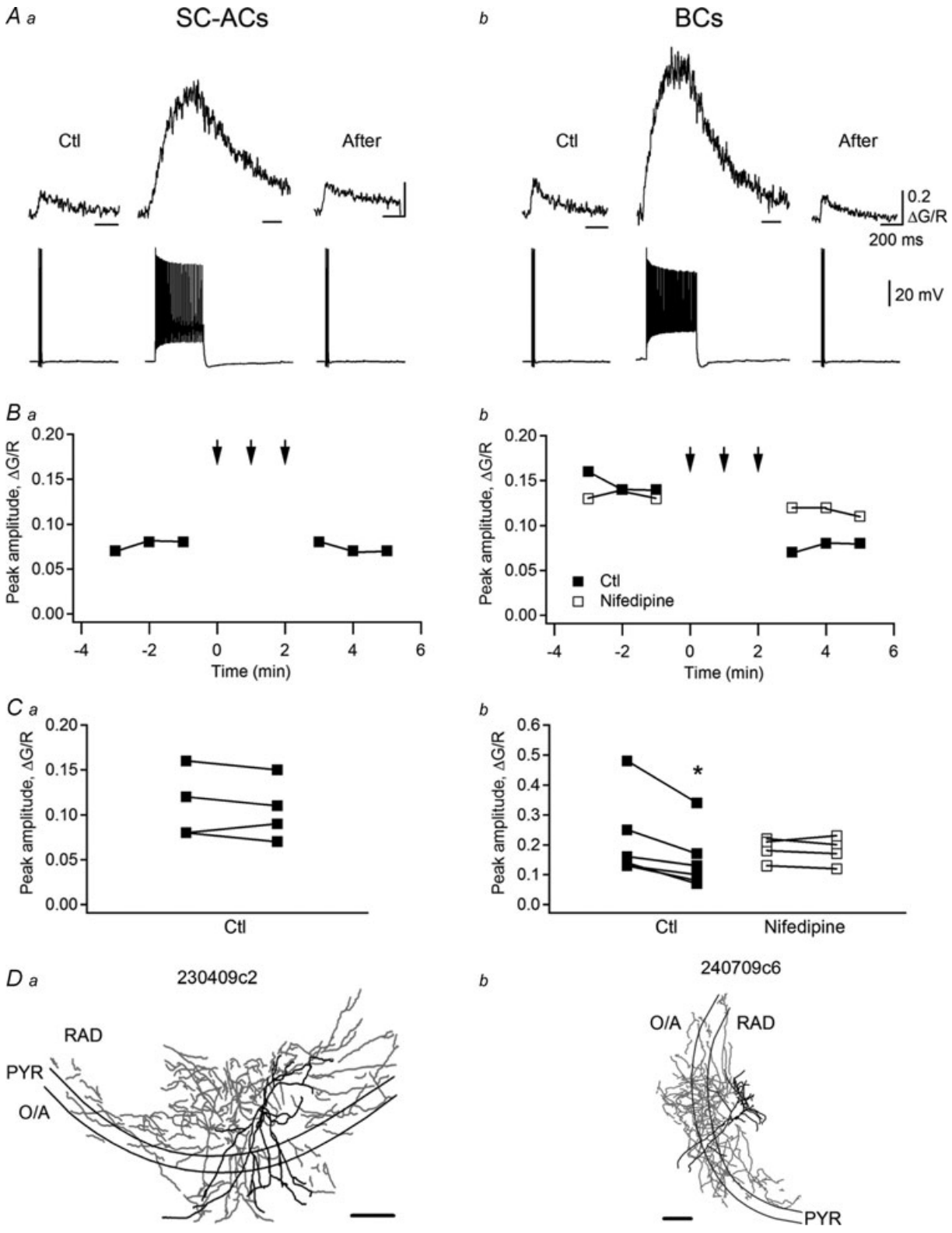

Figure 6. Activity-dependent depression of action potential-evoked Ca^{2+} transients in dendrites of BCs
A, sample traces of AP-CaTs (average of three) evoked by a burst of three APs before (Ctl) and after (After) AP trains (65 Hz, 0.5 s) in an SC-AC (*Aa*) and a BC (*Ab*). *B*, representative data showing the depression of AP-CaTs selectively in BCs (*Bb*) and its absence in SC-ACs (*Ba*). Note that the depression of AP-CaT in BCs was not observed in the presence of the L-type VSCC blocker nifedipine (10 μM). Arrows indicate the periods of time during which

in different cell types, as well as the dynamic profile of Ca^{2+} fluctuations during physiologically relevant patterns of neuronal activity, remain elusive. This study identified the activity-dependent properties of dendritic Ca^{2+} rises in two distinct types of CA1 RAD INs: regularly spiking BCs and SC-ACs. Our major finding is that the same patterns of activity in BCs and SC-ACs translate into differential Ca^{2+} signals in their dendrites. In BCs, AP-evoked Ca^{2+} rises exhibited a relatively large amplitude and fast kinetics. A single AP in these cells raises dendritic $[Ca^{2+}]$ to ∼100–500 nM, which returns to the baseline within ∼40 ms. In SC-ACs, AP-evoked Ca^{2+} transients are significantly smaller and slower, reaching ∼40–200 nM and returning to the baseline within ∼60 ms. These differences between the two cell types are mediated by distinct endogenous Ca^{2+} binding capacities: ∼70 in BCs *vs.* ∼170 in SC-ACs.

Ca^{2+} binding protein calbindin expressed by both SC-ACs and BCs has been shown to undergo a rapid wash-out during whole-cell recordings (Zhou & Neher, 1993; Müller *et al.* 2005) and, thus, cannot contribute to distinct endogenous Ca^{2+} binding capacities found in these cells. Therefore, the observed difference in the endogenous Ca^{2+} buffering may result from differential expression of immobile Ca^{2+} buffers, including Ca^{2+} extrusion mechanisms such as plasma-membrane Ca^{2+} pumps, SERCA, the mitochondrial uniporter and the Na^+/Ca^{2+} exchanger. The molecular identity of these mechanisms and their cell type-specific expression remain to be determined in the future studies.

Overall, AP-evoked Ca^{2+} rises in the two types of INs examined here were lower and slower than those detected in the dendrites of pyramidal cells ($[Ca^{2+}]$: ∼0.4–2 μM; τ_{decay}: ∼21 ms; Sabatini *et al.* 2002); however, they were larger and faster than those observed in fast-spiking (FS) BCs ($[Ca^{2+}]$: ∼0.04 μM; τ_{decay}: ∼200 ms; Aponte *et al.* 2008). Therefore, although the comparison between AP-CaT values obtained here for regularly spiking INs and those for FS-BCs (Aponte *et al.* 2008) is not entirely appropriate because of the different imaging approaches used in these studies, the data suggest that, based on the amplitude and the speed of the decay of AP-CaTs, two types of regularly spiking CA1 INs may be positioned between pyramidal neurons and fast-spiking basket cells: PYRs > RS-BCs > SC-ACs > FS-BCs. Importantly, the properties of AP-evoked Ca^{2+} signals differed significantly between the two types of BCs: RS (expressing CCK) and FS (expressing PV). This can be related directly to the highly specific functions played by these cells in hippocampal circuitry. FS-BCs represent fast inhibitory devices providing a very rapid and temporally precise inhibition with synchronous GABA release (Kraushaar & Jonas, 2000), whereas RS-BCs integrate multiple inputs over time and exhibit asynchronous release (Hefft & Jonas, 2005). The two release modes may exhibit differential Ca^{2+} dependence, which indicates the existence of two distinct types of Ca^{2+} sensors (Sun *et al.* 2007; Kerr *et al.* 2008; Daw *et al.* 2009). However, given that asynchronous release increases rapidly with increasing $[Ca^{2+}]$ (Daw *et al.* 2009), the significantly higher Ca^{2+} rises produced by APs in RS-BCs could account partly for the asynchronous release at RS-BC synapses. Yet, the magnitude of Ca^{2+} elevations in axonal terminals of RS-BCs may not be similar to those occurring in dendrites; this remains to be determined.

In dendrites of most inhibitory INs, AP-evoked Ca^{2+} rises attenuate significantly with distance from the soma because of a higher density of K^+ channels in distal dendrites (Kaiser *et al.* 2001; Goldberg *et al.* 2003; Aponte *et al.* 2008; Topolnik *et al.* 2009; Hu *et al.* 2010; but see Rozsa *et al.* 2004). In agreement with previous studies, our data also revealed a significant decline in the amplitude of AP-evoked Ca^{2+} elevations along the dendritic tree in both BCs and SC-ACs of mouse hippocampus. However, these findings are in disaccord with the incremental scaling of AP-CaTs reported by Rozsa *et al.* (2004) in a population of CA1 RAD INs of rat hippocampus. Unfortunately, no attempt was made to identify the recorded INs in that study (Rozsa *et al.* 2004), and the cellular identity of the INs that demonstrated a distance-dependent increment of AP-CaTs remains unknown. In our study, the distance dependence of AP-evoked Ca^{2+} rises was explored in 35 INs of different subtypes (including BCs, SC-ACs, bistratified and trilaminar cells and some unidentified INs with complex axonal arborizations) in the CA1 RAD. All recorded INs demonstrated a distance-dependent decline in AP-CaT amplitude, suggesting that the interneuron-type-specific properties of dendritic organization do not explain these divergent results. Alternatively, differences in experimental conditions (rats *vs.* mice, room *vs.* physiological temperature, number of APs and/or different diameter of pipette tips (Pusch & Neher, 1988; Oliva *et al.* 1988) and access resistance, which are important for dye diffusion and equilibration (Yasuda *et al.* 2004)) may account for the discrepancy observed.

AP trains were applied. *C*, summary data for a population of cells showing the effect of AP trains on AP-CaTs' amplitude in the dendrites of SC-ACs (*Ca*) and BCs (*Cb*). Experiments were performed using Fluo-5F as a Ca^{2+} indicator. *D*, Neurolucida reconstructions of two representative INs from which the recordings were obtained. Scale bars, 200 μm.

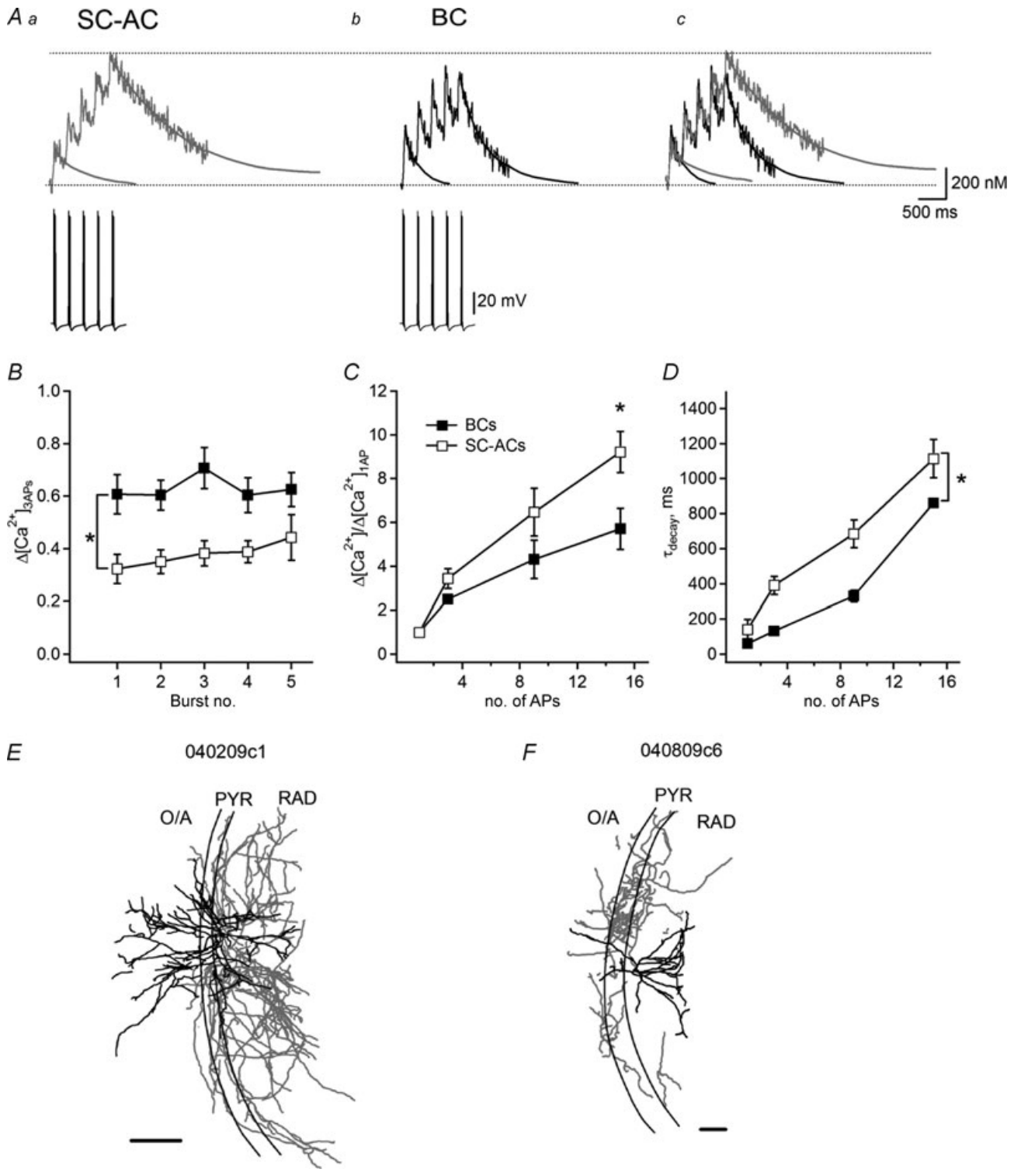

Figure 7. Temporal summation of action potential-evoked Ca^{2+} transients during theta bursting
A, representative examples of AP-CaTs (average of three; top) recorded using Fluo-5F in the dendrites of SC-ACs (*Aa*) and BCs (*Ab*), as well as their superimposition (*Ac*) in response to five bursts of three APs applied at a 4 Hz frequency (bottom). *B*, summary plot showing the amplitude of $\Delta[Ca^{2+}]_{3APs}$ evoked by individual bursts in the two cell types. *C*, summary plot showing a degree of summation of $\Delta[Ca^{2+}]_{3APs}$ during continuous bursting in dendrites of the two cell types. Note a higher summation level in SC-ACs. *D*, summary plot demonstrating changes in τ_{decay} of $\Delta[Ca^{2+}]_{3APs}$ during continuous bursting in the two cell types. $^*P < 0.05$, ANOVA. *E–F*, Neurolucida reconstructions of two representative biocytin-filled INs from which the recordings were obtained. Scale bars, 200 μm.

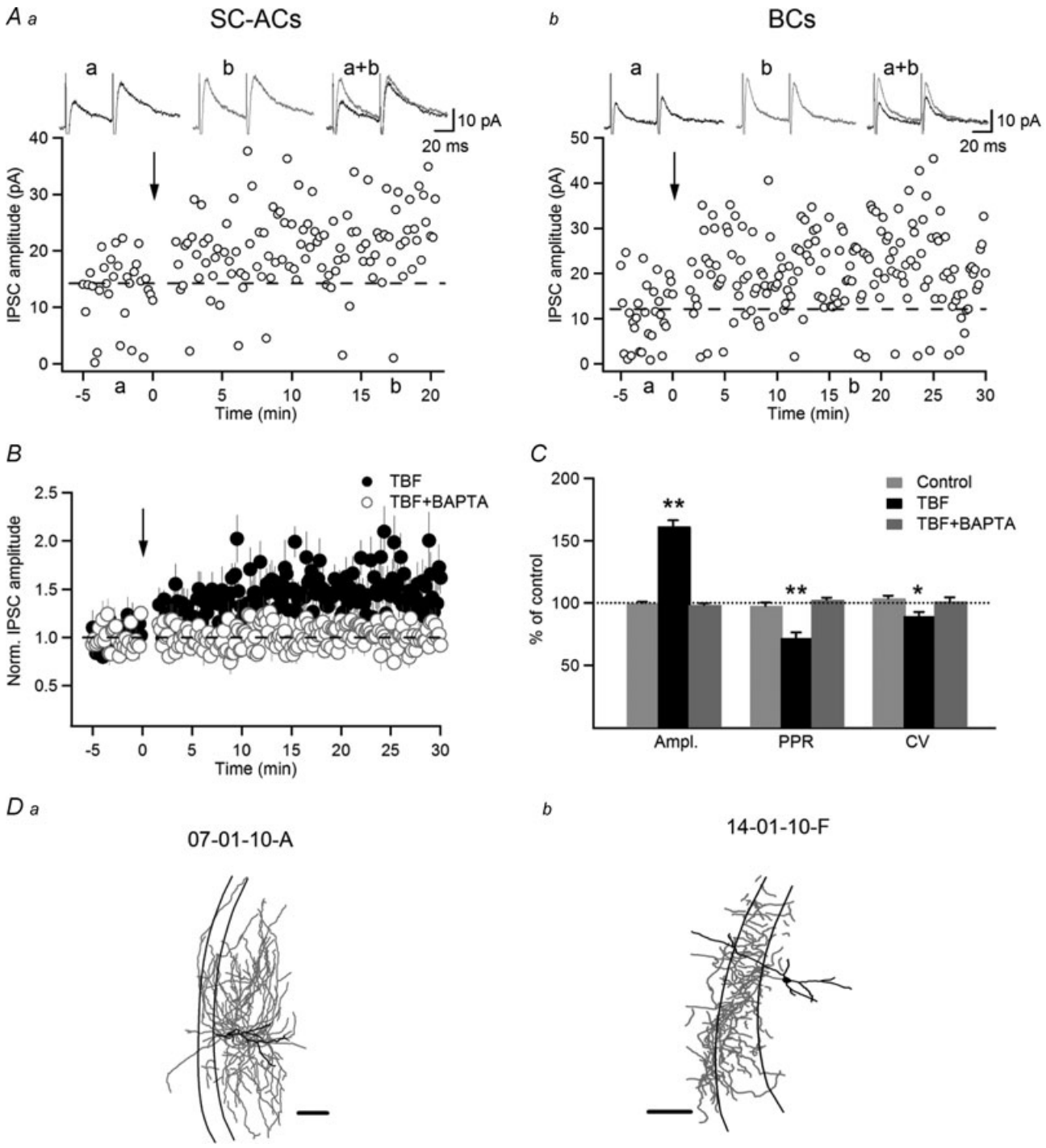

Figure 8. Theta-burst firing induced LTP at inhibitory synapses onto both SC-ACs and BCs
A, representative examples of IPSC amplitudes *vs.* time in SC-AC (*Aa*) and BC (*Ab*), showing LTP of IPSCs induced by TBF in the two cell types. The traces at the top are average IPSCs (average of 30 sweeps, failures included) in a control setting (*a*), 20 min after TBF (*b*) and their superimposition. *B*, normalized group data showing LTP in control (black symbols; $n = 7$) and its absence when BAPTA (10 mM) was included in the recording solution (red symbols; $n = 4$). *C*, summary bar graphs showing changes in the IPSC peak amplitude, PPR and CV induced by TBF. The LTP of IPSCs was associated with a significant decrease in PPR and CV, indicating a presynaptic locus for its expression. *D*, Neurolucida reconstructions of the two representative biocytin-filled INs that were used to obtain the recordings depicted in *A*. Scale bars, 100 μm. The error bars throughout represent the SEM.

Cell type-specific mechanisms and regulation of Ca^{2+} transients

The results of the present study also revealed the cell type-specific mechanisms of AP-CaTs in RAD INs. T-type VSCCs mediated 39.6 ± 4.1% of AP-CaTs in SC-ACs and only 20.5 ± 5.7% of AP-CaTs in BCs. In contrast, P/Q-type VSCCs contributed to 28.2 ± 3.4% of AP-CaTs in BCs and did not participate in AP-CaTs in SC-ACs. Accordingly, the AP-CaT amplitude in IN dendrites was differentially affected by the level of membrane potential from which the APs were generated. In SC-ACs, AP-CaTs were significantly increased by membrane hyperpolarization due to enhanced contribution of T-type VSCCs, which could result from the channel recovery from the inactivation state at −80 mV (McRory *et al.* 2001; Carter & Sabatini, 2004). T-type VSCCs contribute to dendritic Ca^{2+} signals in pyramidal cells (Magee *et al.* 1995), granule cells of the olfactory bulb (Egger *et al.* 2003), Purkinje cells (Mouginot *et al.* 1997) and cortical and hippocampal INs (Goldberg *et al.* 2004; Topolnik *et al.* 2009). Consistent with previous findings regarding the expression of the Cav3.1 subunit of T-type VSCCs in CCK-IR CA1 INs (Vinet & Sík, 2006), the results of the present study indicate that these channels contribute to AP-CaTs in both BCs and SC-ACs. However, the higher contribution of T-type VSCCs in dendrites of SC-ACs together with their membrane-potential-dependent recruitment suggests that these channels may preferentially shape the dynamics of AP-CaTs in SC-ACs. In contrast, in BCs, AP-CaTs were decreased with membrane hyperpolarization. In this case, the membrane-potential-induced regulation of AP-CaTs progressed independently of the T-type VSCCs, but was associated with a decreased availability of L-type VSCCs and, possibly, of P/Q-type VSCCs at −80 mV. L-type VSCCs contribute to AP-CaTs in hippocampal INs (Topolnik *et al.* 2009) and both Cav1.2 and Cav1.3 subunits are expressed in CCK-IR cells (although the Cav1.2 was detected only in half the CCK-IR cells; Vinet & Sík, 2006). Given the channel activation profile, it is unlikely that it contributes significantly to AP-CaTs at −80 mV, as was apparent from present results in BCs. These findings are in agreement with previous results obtained in striatal medium spiny neurons (Carter & Sabatini, 2004), which also indicate the presence of a membrane-potential-dependent regulation of AP-CaTs in relation to different states of network (up state *vs.* down state).

From the experiments presented here, it appears that following high-frequency firing episodes in the gamma band AP-CaTs are significantly depressed selectively in BCs. A similar activity-dependent depression of AP-CaTs after relatively brief firing episodes (63 Hz, 0.5 s) occurs in dendritic spines of pyramidal cells and interferes with the induction of long-term synaptic plasticity (Yasuda *et al.* 2003). Induction of AP-CaT depression in pyramidal neurons is Ca^{2+} dependent and requires Ca^{2+} influx via L-type VSCCs, activation of the Ca^{2+}/calmodulin-dependent kinase II (CaMKII) and a cAMP-dependent pathway. AP-CaT depression is expressed as a decrease in the open probability of R-type VSCCs. While L-type VSCCs are expressed at high density in CCK-IR GABAergic INs, the Cav1.2 exhibits a cell type-specific distribution (Vinet & Sík, 2006). Furthermore, αCaMKII, found in pyramidal cells, is not detected in inhibitory INs (Liu & Jones, 1996; Sík *et al.* 1998) and appears to be replaced by a different isoform (Lamsa *et al.* 2007). Thus, it was unclear whether L-type VSCC/CaMKII/cAMP-dependent depression of AP-CaTs may be induced in IN dendrites by brief episodes of high-frequency firing. The results of the present study revealed a cell type-specific depression of AP-CaTs controlled by L-type VSCCs, pointing to a fulfilment of all required conditions for its specific induction in BCs. The lack of AP-CaT depression in SC-ACs, which express L-type VSCCs, could be due to a different organization of L-type/Ca^{2+}-dependent signalling cascade, thereby interfering with the induction of this form of plasticity. In this study, no attempt was made to determine possible cell type-specific mechanisms of this form of dendritic plasticity and its consequences in synaptic plasticity, which will have to be addressed in the future.

Role of action potential-evoked dendritic Ca^{2+} transients in plasticity at IN inhibitory synapses

Our data also indicate that the smaller and slower AP-CaTs found in the dendrites of SC-ACs compared with those detected in BCs were amplified significantly during theta-like activity as a result of a more efficient temporal summation of AP-CaTs in SC-ACs; this suggests that the quantitatively different Ca^{2+} rises recorded in the two cell types under basal conditions can be essentially normalized by changes in neuron activity. Overall efficient temporal summation of AP-CaTs during theta-burst firing in both SC-ACs and BCs resulted in the induction of LTP at inhibitory synapses onto these cells. These data suggest that under natural conditions theta episodes can be associated with an increase in the inhibition of CCK-expressing INs and a subsequent disinhibition of principal cells. This downregulation of the inhibition may be necessary for the efficient integration of excitatory inputs by place cells supporting their firing and resulting in the induction of a short-term depression of CCK inhibitory inputs via release of endocannabinoids (Katona *et al.* 1999). Accordingly, theta oscillations may be associated with an overall decrease in inhibition originating from the CCK-expressing INs, which can be

particularly important in sparse coding by place cells (Klausberger *et al.* 2005).

LTP at inhibitory synapses onto both SC-ACs and BCs was induced postsynaptically, as it was triggered by postsynaptic firing alone and required postsynaptic Ca^{2+} elevation. However, the expression locus of this LTP was located at the presynaptic site, suggesting the implication of a retrograde signal. Although no attempt was made in the current study to investigate the mechanisms of LTP induction, nitric oxide (NO) or brain-derived neurotrophic factor (BDNF) may be involved in this presynaptic LTP. The Ca^{2+}-dependent neuronal NO synthase is expressed in calbindin-positive INs (Jinno & Kosaka, 2002). NO synthesis is tightly controlled by intracellular Ca^{2+} elevation, so that as little as 250–350 nM of Ca^{2+} is sufficient to trigger the production of NO (Bredt & Snyder, 1990; Pollock *et al.* 1991). Furthermore, an NO-dependent form of LTP was identified at inhibitory synapses onto dopaminergic neurons of the ventral tegmental area (Nugent *et al.* 2007). Whether this form of presynaptic plasticity represents a common mechanism of regulation of inhibitory synapses remains to be determined. As for BDNF, a role for this molecule in the LTP expressed presynaptically was reported at inhibitory synapses onto CA3 pyramidal cells early during development, although dendritic synthesis of BDNF required a significantly higher stimulation protocol (depolarizing pulses of 500 ms) and, accordingly, higher Ca^{2+} elevations (Caillard *et al.* 1999; Kuczewski *et al.* 2008). Remarkably, in our study, BCs and SC-ACs (as well as one bistratified cell; S. Chamberland & L. Topolnik, unpublished data) exhibited this form of inhibitory synapse plasticity, demonstrating the presence of a fairly universal form of LTP at inhibitory synapses of RAD INs.

In conclusion, the results presented here favour a model in which AP-evoked dendritic Ca^{2+} rises fluctuate continuously and are dependent on IN state and activity pattern. These dynamic $[Ca^{2+}]$ fluctuations are controlled by the basic Ca^{2+} handling properties of INs and by the distribution and availability of particular Ca^{2+} sources and/or Ca^{2+} extrusion mechanisms in different cell types. Given that the state and/or the availability of Ca^{2+} mechanisms control the induction of synaptic plasticity, cell type-specific dynamics of Ca^{2+} signalling will determine the rules of the induction of cell type-specific forms of plasticity. Conversely, the interneuron-specific differences in AP-evoked dendritic Ca^{2+} signals can be essentially 'smoothed out' by changes in neuronal activity, so that Ca^{2+} signals of similar profile will be produced in different cell types, leading to the induction of common, cell-type-independent forms of synaptic plasticity. Therefore, given that dendritic Ca^{2+} mechanisms represent a highly dynamic entity (Yasuda *et al.* 2003; Topolnik *et al.* 2009; present study), the history of neuron activity can be stored in dendrites via dynamically regulated Ca^{2+} signals, thus having a profound effect on the integration of synaptic inputs.

References

Ali AB (2007). Presynaptic inhibition of $GABA_A$ receptor-mediated unitary IPSPs by cannabinoid receptors at synapses between CCK-positive interneurons in rat hippocampus. *J Neurophysiol* **98**, 861–869.

Aponte Y, Bischofberger J & Jonas P (2008). Efficient Ca^{2+} buffering in fast-spiking basket cells of rat hippocampus. *J Physiol* **586**, 2061–2075.

Bragin A, Jandó G, Nádasdy Z, van Landeghem M & Buzsáki G (1995). Dentate EEG spikes and associated interneuronal population bursts in the hippocampal hilar region of the rat. *J Neurophysiol* **73**, 1691–1705.

Bredt DS & Snyder SH (1990). Isolation of nitric oxide synthetase, a calmodulin-requiring enzyme. *Proc Natl Acad Sci U S A* **87**, 682–685.

Caillard O, Ben-Ari Y & Gaiarsa JL (1999). Long-term potentiation of GABAergic synaptic transmission in neonatal rat hippocampus. *J Physiol* **518**, 109–119.

Callaway JC & Ross WN (1995). Frequency-dependent propagation of sodium action potentials in dendrites of hippocampal CA1 pyramidal neurons. *J Neurophysiol* **74**, 1395–1403.

Carter AG & Sabatini BL (2004). State-dependent calcium signaling in dendritic spines of striatal medium spiny neurons. *Neuron* **44**, 483–493.

Cope DW, Maccaferri G, Márton LF, Roberts JD, Cobden PM & Somogyi P (2002). Cholecystokinin-immunopositive basket and Schaffer collateral-associated interneurones target different domains of pyramidal cells in the CA1 area of the rat hippocampus. *Neuroscience* **109**, 63–80.

Csicsvari J, Hirase H, Czurko A & Buzsáki G (1998). Reliability and state dependence of pyramidal cell-interneuron synapses in the hippocampus: an ensemble approach in the behaving rat. *Neuron* **21**, 179–189.

Daw MI, Tricoire L, Erdelyi F, Szabo G & McBain CJ (2009). Asynchronous transmitter release from cholecystokinin-containing inhibitory interneurons is widespread and target-cell independent. *J Neurosci* **29**, 11112–11122.

Denk W, Sugimori M & Llinás R (1995). Two types of calcium response limited to single spines in cerebellar Purkinje cells. *Proc Natl Acad Sci U S A* **92**, 8279–8282.

Egger V, Svoboda K & Mainen ZF (2003). Mechanisms of lateral inhibition in the olfactory bulb: efficiency and modulation of spike-evoked calcium influx into granule cells. *J Neurosci* **23**, 7551–7558.

Goldberg JH, Yuste R & Tamas G (2003). Ca^{2+} imaging of mouse neocortical interneuron dendrites: Ia type K^+ channels control action potential backpropagation. *J Physiol* **551**, 49–65.

Goldberg JH, Lacefield CO & Yuste R (2004). Global dendritic calcium spikes in mouse layer 5 low threshold spiking interneurones: implications for control of pyramidal cell bursting. *J Physiol* **558**, 465–478.

Gulyas AI, Megias M, Emri Z & Freund TF (1999). Total number and ratio of excitatory and inhibitory synapses converging onto single interneurons of different types in the CA1 area of the rat hippocampus. *J Neurosci* **19**, 10082–10097.

Hefft S & Jonas P (2005). Asynchronous GABA release generates long-lasting inhibition at a hippocampal interneuron-principal neuron synapse. *Nat Neurosci* **8**, 1319–1328.

Helmchen F, Imoto K & Sakmann B (1996). Ca^{2+} buffering and action potential-evoked Ca^{2+} signaling in dendrites of pyramidal neurons. *Biophys J* **70**, 1069–1081.

Hu H, Martina M & Jonas P (2010). Dendritic mechanisms underlying rapid synaptic activation of fast-spiking hippocampal interneurons. *Science* **327**, 52–58.

Huang L, Keyser BM, Tagmose TM, Hansen JB, Taylor JT, Zhuang H, Zhang M, Ragsdale DS & Li M (2004). NNC 55-0396 [(1S,2S)-2-(2-(N-[(3-benzimidazol-2-yl)propyl]-N-methylamino)ethyl)-6-fluoro-1,2,3,4-tetrahydro-1-isopropyl-2-naphtyl cyclopropanecarboxylate dihydrochloride]: a new selective inhibitor of T-type calcium channels. *J Pharmacol Exp Ther* **309**, 193–199.

Jinno S & Kosaka T (2002). Patterns of expression of calcium binding proteins and neuronal nitric oxide synthase in different populations of hippocampal GABAergic neurons in mice. *J Comp Neurol* **449**, 1–25.

Katona I, Sperlagh B, Sík A, Kafalvi A, Vizi ES, Mackie K & Freund TF (1999). Presynaptically located CB1 cannabinoid receptors regulate GABA release from axon terminals of specific hippocampal interneurons. *J Neurosci* **19**, 4544–4558.

Kaiser KM, Zilberter Y & Sakmann B (2001). Back-propagating action potentials mediate calcium signalling in dendrites of bitufted interneurons in layer 2/3 of rat somatosensory cortex. *J Physiol* **535**, 17–31.

Kerr AM, Reisinger E & Jonas P (2008). Differential dependence of phasic transmitter release on synaptotagmin 1 at GABAergic and glutamatergic hippocampal synapses. *Proc Natl Acad Sci U S A* **105**, 15581–15586.

Klausberger T, Magill P, Márton LF, Roberts JD, Cobden PM, Buzsáki G & Somogyi P (2003). Brain-state- and Cell type-specific firing of hippocampal interneurons *in vivo*. *Nature* **421**, 844–848.

Klausberger T, Marton LF, O'Neill J, Huck JHJ, Dalezios Y, Fuentealba P, Suen WY, Papp E, Kaneko T, Watanabe M, Csicsvari J & Somogyi P (2005). Complementary roles of cholecystokinin- and parvalbumin- expressing GABAergic neurons in hippocampal network oscillations. *J Neurosci* **25**, 9782–9793.

Klausberger T (2009). GABAergic interneurons targeting dendrites of pyramidal cells in the CA1 area of the hippocampus. *Eur J Neurosci* **30**, 947–957.

Kraushaar U & Jonas P (2000). Efficacy and stability of quantal GABA release at a hippocampal interneuron-principal neuron synapse. *J Neurosci* **20**, 5594–5607.

Kuczewski N, Porcher C, Ferrand N, Fiorentino H, Pellegrino C, Kolarow R, Lessmann V, Medina I & Gaiarsa JL (2008). Backpropagating action potentials trigger dendritic release of BDNF during spontaneous network activity. *J Neurosci* **28**, 7013–7023.

Lamsa KP, Heeroma JH & Kullmann DM (2005). Hebbian LTP in feed-forward inhibitory interneurons and the temporal fidelity of input discrimination. *Nat Neurosci* **8**, 916–924.

Lamsa K, Irvine EE, Giese KP & Kullmann DM (2007). NMDA receptor-dependent long-term potentiation in mouse hippocampal interneurons shows a unique dependence on Ca^{2+}/calmodulin-dependent kinases. *J Physiol* **584**, 885–894.

Lapointe V, Morin F, Ratte S, Croce A, Conquet F & Lacaille J-C (2004). Synapse-specific mGluR1-dependent long-term potentiation in interneurones regulates mouse hippocampal inhibition. *J Physiol* **15**, 125–135.

Lee SH, Rosenmund C, Schwaller B & Neher E (2000). Differences in Ca^{2+} buffering properties between excitatory and inhibitory hippocampal neurons from the rat. *J Physiol* **525**, 405–418.

Lei S & McBain CJ (2002). Distinct NMDA receptors provide differential modes of transmission at mossy fiber-interneuron synapses. *Neuron* **33**, 921–933.

Li M, Hansen JB, Huang L, Keyser BM & Taylor JT (2005). Towards selective antagonists of T-type calcium channels: design, characterization and potential applications of NNC 55-0396. *Cardiovasc Drug Rev* **23**, 173–196.

Liu XB & Jones EG (1996). Localization of α type II calcium calmodulin-dependent protein kinase at glutamatergic but not γ-aminobutyric acid (GABAergic) synapses in thalamus and cerebral cortex. *Proc Natl Acad Sci U S A* **93**, 7332–7336.

Magee JC, Christofi G, Miyakawa H, Christie B, Lasser-Ross N & Johnston D (1995). Subthreshold synaptic activation of voltage-gated Ca^{2+} channels mediates a localized Ca^{2+} influx into the dendrites of hippocampal pyramidal neurons. *J Neurophysiol* **74**, 1335–1342.

Maravall M, Mainen ZF, Sabatini BL & Svoboda K (2000). Estimating intracellular calcium concentrations and buffering without wavelength ratioing. *Biophys J* **78**, 2655–2667.

Martina M, Vida I & Jonas P (2000). Distal initiation and active propagation of action potentials in interneuron dendrites. *Science* **287**, 295–300.

McRory JE, Santi CM, Hamming KS, Mezeyova J, Sutton KG, Baillie DL, Stea A & Snutch TP (2001). Molecular and functional characterization of a family of rat brain T-type calcium channels. *J Biol Chem* **276**, 3999–4011.

Mouginot D, Bossu JL & Gähwiler BH (1997). Low-threshold Ca^{2+} currents in dendritic recordings from Purkinje cells in rat cerebellar slice cultures. *J Neurosci* **17**, 160–170.

Müller A, Kukley M, Stausberg P, Beck H, Müller W & Dietrich D (2005). Endogenous Ca^{2+} buffer concentration and Ca^{2+} microdomains in hippocampal neurons. *J Neurosci* 25, 558–565.

Neher E & Augustine GJ (1992). Calcium gradients and buffers in bovine chromaffin cells. *J Physiol* **450**, 273–301.

Nugent FS, Penick EC & Kauer JA (2007). Opioids block long-term potentiation of inhibitory synapses. *Nature* **446**, 1086–1090.

O'Keefe J & Recce ML (1993). Phase relationship between hippocampal place units and the EEG theta rhythm. *Hippocampus* **3**, 317–330.

Oliva C, Cohen IS & Mathias RT (1988). Calculation of time constants for intracellular diffusion in whole cell patch clamp configuration. *Biophys J* **54**, 791–799.

Patenaude C, Massicotte G & Lacaille JC (2005). Cell-type specific GABA synaptic transmission and activity-dependent plasticity in rat hippocampal stratum radiatum interneurons. *Eur J Neurosci* **22**, 179–188.

Pawelzik H, Hughes DI & Thomson AM (2002). Physiological and morphological diversity of immunocytochemically defined parvalbumin- and cholecystokini-positive interneurons in CA1 of the adult rat hippocampus. *J Comp Neurol* **443**, 346–367.

Perez Y, Morin F & Lacaille JC (2001). A hebbian form of long-term potentiation dependent on mGluR1a in hippocampal inhibitory interneurons. *Proc Natl Acad Sci U S A* **98**, 9401–9406.

Pettit DL & Augustine GJ (2000). Distribution of functional glutamate and GABA receptors on hippocampal pyramidal cells and interneurons. *J Neurophysiol* **84**, 28–38.

Pusch M & Neher E (1988). Rates of diffusional exchange between small cells and a measuring patch pipette. *Pflugers Arch* **411**, 204–211.

Rozsa B, Zelles T, Vizi ES & Lendvai B (2004). Distance-dependent scaling of calcium transients evoked by backpropagating spikes and synaptic activity in dendrites of hippocampal interneurons. *J Neurosci* **24**, 661–670.

Sabatini B & Svoboda K (2000). Analysis of calcium channels in single spines using optical fluctuation analysis. *Nature* **408**, 589–593.

Sabatini BL, Oertner TG & Svoboda K (2002). The life cycle of Ca^{2+} ions in dendritic spines. *Neuron* **33**, 439–452.

Scheuss V, Yasuda R, Sobczyk A & Svoboda K (2006). Nonlinear $[Ca^{2+}]$ signaling in dendrites and spines caused by activity-dependent depression of Ca^{2+} extrusion. *J Neurosci* **26**, 8183–8194.

Pollock JS, Förstermann U, Mitchell JA, Warner TD, Schmidt HH, Nakane M & Murad F (1991). Purification and characterization of particulate endothelium-derived relaxing factor synthase from cultured and native bovine aortic endothelial cells. *Proc Natl Acad Sci U S A* **88**, 10480–10484.

Sík A, Hájos N, Gulácsi A, Mody I & Freund TF (1998). The absence of a major Ca^{2+} signaling pathway in GABAergic neurons of the hippocampus. *Proc Natl Acad Sci U S A* **95**, 3245–3250.

Soltesz I & Deschênes M (1993). Low- and high-frequency membrane potential oscillations during theta activity in CA1 and CA3 pyramidal neurons of the rat hippocampus under ketamine-xylazine anesthesia. *J Neurophysiol* **70**, 97–116.

Sun J, Pang ZP, Qin D, Fahim AT, Adachi R & Südhof TC (2007). A dual-Ca^{2+}-sensor model for neurotransmitter release in a central synapse. *Nature* **450**, 676–682.

Topolnik L, Azzi M, Morin F, Kougiuomoutzakis A & Lacaille JC (2006). mGluR1/5 subunit-specific Ca^{2+} signalling and long-term potentiation in rat hippocampal oriens/alveus interneurons. *J Physiol* **575**, 115–131.

Topolnik L, Chamberland S, Pelletier JG, Ran I & Lacaille JC (2009). Activity-dependent compartmentalized regulation of dendritic Ca^{2+} signaling in hippocampal interneurons. *J Neurosci* **29**, 4658–4663.

Vida I, Halasy K, Szinyei C, Somogyi P & Buhl EH (1998). Unitary IPSPs evoked by interneurons at the stratum radiatum–stratum lacunosum-moleculare border in the CA1 area of the rat hippocampus *in vitro*. *J Physiol* **506**, 755–773.

Vinet J & Sík A (2006). Expression pattern of voltage-dependent calcium channel subunits in hippocampal inhibitory neurons in mice. *Neuroscience* **143**, 189–212.

Woodruff ML, Sampath AP, Matthews HR, Krasnoperova NV, Lem J & Fain GL (2002). Measurement of cytoplasmic calcium concentration in the rods of wild-type and transducin knock-out mice. *J Physiol* **542**, 843–854.

Yasuda R, Sabatini BL & Svoboda K (2003). Plasticity of calcium channels in dendritic spines. *Nat Neurosci* **6**, 948–955.

Yasuda R, Nimchinsky EA, Scheuss V, Pologruto TA, Oertner TG, Sabatini BL & Svoboda K (2004). Imaging calcium concentration dynamics in small neuronal compartments. *Sci STKE* **219**, l5.

Yuste R & Denk W (1995). Dendritic spines as basic functional units of neuronal integration. *Nature* **375**, 682–684.

Zhou Z & Neher E (1993). Mobile and immobile calcium buffers in bovine adrenal chromaffin cells. *J Physiol* **469**, 245–273.

Author contributions

A.E. and S.C. collected the data and took part in the analysis of results and preparation of Figs 1, 4 and 8. L.T. designed the experiments, analysed the data and wrote the manuscript. All authors approved the final version of the manuscript for publication.

Acknowledgements

We thank Dimitry Topolnik for excellent technical assistance and cells' reconstruction. This work was supported by the Canadian Institutes of Health Research, Natural Sciences and Engineering Research Council of Canada (NSERC Discovery Grant) and Savoy Foundation. L.T. is a recipient of the University Faculty Award from NSERC. S.C. was supported by a fellowship from the Fonds de la Recherche en Santé du Québec.